(12)

TECHNICAL REPORT ARBRL-TR-02470

(Supersedes IMR No. 754)

MOMENT ON A LIQUID-FILLED SPINNING AND NUTATING PROJECTILE: SOLID BODY ROTATION

Nathan Gerber
Raymond Sedney

February 1983

US ARMY ARMAMENT RESEARCH AND DEVELOPMENT COMMAND
BALLISTIC RESEARCH LABORATORY
ABERDEEN PROVING GROUND, MARYLAND

Destroy this report when it is no longer needed.
Do not return it to the originator.

Additional copies of this report may be obtained from the National Technical Information Service, U. S. Department of Commerce, Springfield, Virginia 22161.

The findings in this report are not to be construed as an official Department of the Army position, unless so designated by other authorized documents.

The use of trade names or manufacturers' names in this report does not constitute indorsement of any commercial product.

UNCLASSIFIED

SECURITY CLASSIFICATION OF THIS PAGE *(When Data Entered)*

REPORT DOCUMENTATION PAGE		READ INSTRUCTIONS BEFORE COMPLETING FORM
1. REPORT NUMBER TECHNICAL REPORT ARBRL-TR-02470	2. GOVT ACCESSION NO. AD-A125 332	3. RECIPIENT'S CATALOG NUMBER
4. TITLE *(and Subtitle)* MOMENT ON A LIQUID-FILLED SPINNING AND NUTATING PROJECTILE: SOLID BODY ROTATION		5. TYPE OF REPORT & PERIOD COVERED Final 6. PERFORMING ORG. REPORT NUMBER
7. AUTHOR(s) Nathan Gerber Raymond Sedney		8. CONTRACT OR GRANT NUMBER(s)
9. PERFORMING ORGANIZATION NAME AND ADDRESS US Army Ballistic Research Laboratory ATTN: DRDAR-BLL Aberdeen Proving Ground, Maryland 21005		10. PROGRAM ELEMENT, PROJECT, TASK AREA & WORK UNIT NUMBERS RDT&E 1L161102AH43
11. CONTROLLING OFFICE NAME AND ADDRESS US Army Armament Research & Development Command US Army Ballistic Research Laboratory (DRDAR-BL) Aberdeen Proving Ground, Maryland 21005		12. REPORT DATE February 1983 13. NUMBER OF PAGES 57
14. MONITORING AGENCY NAME & ADDRESS*(if different from Controlling Office)*		15. SECURITY CLASS. *(of this report)* Unclassified 15a. DECLASSIFICATION/DOWNGRADING SCHEDULE

16. DISTRIBUTION STATEMENT *(of this Report)*

Approved for public release, distribution unlimited.

17. DISTRIBUTION STATEMENT *(of the abstract entered in Block 20, if different from Report)*

18. SUPPLEMENTARY NOTES

This report supersedes IMR No. 754, dated October 1982.

19. KEY WORDS *(Continue on reverse side if necessary and identify by block number)*

Linearized Navier-Stokes Equations	Liquid Pressure Moment
Liquid-Filled Gyroscope	Viscous Shear Moment
Liquid-Filled Shell	Rotating Fluid
Liquid Moment	Solid Body Rotation
Liquid Payload	Spinning Nutating Cylinder

20. ABSTRACT *(Continue on reverse side if necessary and identify by block number)* (bja)

The moment exerted on the casing by a completely spun-up liquid filling a spinning and nutating right circular cylinder is evaluated. Among the restrictions of the theory are (1) assumption of small yaw angle, and (2) constant spin and nutational frequencies and timewise exponential yaw growth. The new feature of this work is the inclusion of viscous shear in the liquid force on the cylinder walls. It is found that the viscous shear contributes significantly to

DD FORM 1 JAN 73 1473 EDITION OF 1 NOV 65 IS OBSOLETE

UNCLASSIFIED

SECURITY CLASSIFICATION OF THIS PAGE *(When Data Entered)*

the overturning moment in many instances. Outputs are compared with those of the theory of Murphy, which makes the additional assumption of inviscid flow except for boundary layers near the walls. Results of the two theories agree well for high Reynolds numbers ($\geq 5\times10^4$) but diverge increasingly as Reynolds number is decreased. Comparisons of calculated yaw growth rates are made with measurements taken in gyroscope experiments for aspect-ratios of 1.0 and 3.1. The differences between theory and experiment are greater for the 3.1 aspect-ratio cylinder than for the 1.0 case. The present theory generally shows better agreement with experiment at the lower Reynolds numbers than does the Murphy theory. Both theories demonstrate a strong sensitivity of yaw growth rate to variation in cylinder aspect ratio.

TABLE OF CONTENTS

LIST OF ILLUSTRATIONS

LIST OF ILLUSTRATIONS (Continued)

I. INTRODUCTION

A liquid-filled projectile can become unstable in flight when resonance occurs between the angular motion (nutation) of the shell and certain non-axisymmetric inertial oscillations of the spinning liquid. Theoretical determinations[1, 2, 3] of frequencies of these oscillations (eigenfrequencies), together with their associated decay rates, have been made, mainly for liquids in solid body rotation after completion of spin-up. These stem from the work of Stewartson[4] and Wedemeyer.[5,6] Reference 7 describes flow field pressure measurements made to determine eigenfrequencies experimentally for solid body rotation, and Reference 8 treats measurements made during spin-up from rest.

The next step is to determine the liquid moment acting on the casing and then to predict the angular motion of the projectile. Because of a simplifying approximation* the early predictions of pressure moment[1, 2] were limited to

---

* *The sum of a Laurent series is replaced by a single term; see, e.g., Eq. (5.10) of Reference 4.*

1. *J. T. Frasier and W. E. Scott, "Dynamics of a Liquid-Filled Shell," BRL Report No. 1391, February 1968. AD 667365.*

2. *Engineering Design Handbook, Liquid-Filled Projectile Design, AMC Pamphlet 706-165, April 1969. AD 853719.*

3. *C. W. Kitchens, Jr., N. Gerber, and R. Sedney, "Oscillations of a Liquid in a Rotating Cylinder: Part I. Solid-Body Rotation," BRL Technical Report ARBRL-TR-02081, June 1978. AD A057759.*

4. *K. Stewartson, "On the Stability of a Spinning Top Containing Liquid," J. Fluid Mech., Vol. 5, Part 4, September 1959, pp. 577-592.*

5. *E. H. Wedemeyer, "Dynamics of Liquid-Filled Shell: Theory of Viscous Corrections to Stewartson's Stability Problem," BRL Report 1287, June 1965. AD 472474.*

6. *E. H. Wedemeyer, "Viscous Corrections to Stewartsons's Stability Criterion," BRL Report No. 1325, June 1966. AD 489387.*

7. *R. D. Whiting, "An Experimental Study of Forced Asymmetric Oscillations in a Rotating Liquid-Filled Cylinder," BRL Technical Report ARBRL-TR-02376, October 1981. ADA 107948.*

8. *S. Stergiopoulos, "An Experimental Study of Inertial Waves in a Fluid Contained in a Rotating Cylindrical Cavity During Spin-Up From Rest," PhD. Thesis, York Univeristy, Toronto, Ontario, February 1982.*

nutational frequencies lying close to liquid eigenfrequencies. Two recent studies[9,10] have produced liquid moment calculations valid for all angular frequencies. Reference 9 treats only the pressure moment on completely-filled projectiles using viscous perturbation equations. Reference 10 treats both presssure and viscous shear moments for partially and totally filled projectiles, with and without central rod; this work is an extension of the Stewartson-Wedemeyer theory which employs the inviscid perturbation equations. In this report we extend the analysis of Reference 9, which uses the viscous perturbation equations, to include the shear moment; again, we treat only the filled shell.

There are four basic assumptions in all the studies, including the present one: (1) The angle of yaw is very small, permitting linearization of Navier-Stokes equations and boundary conditions. (2) The projectile is traveling in a straight trajectory, is nutating at a constant rate about a point on its axis, and experiencing exponential yaw growth with time. (3) The initial state of the liquid is solid body rotation at a spin rate that remains unchanged even after the perturbation is applied. (4) The timewise variation of the flow variables is the same as that of the motion of the shell.

Gyroscope experiments[11,12] have provided simultaneous measurements of (1) nutational frequency* τ and (2) yaw growth rate ε, the two parameters that describe the angular motion. Theoretical outputs will be compared with these results.

II. ANGULAR MOTION OF PROJECTILE

Here we summarize Chapters II and VI of Reference 9. Two coordinate systems are considered. The first is an inertial, earth-fixed system of axes x, y, z. The x-axis coincides with the projectile velocity vector, and the z-axis lies in the vertical plane; then the y-axis is directed so as to form a right-handed system. The second system is the aeroballistic $\tilde{x}$, $\tilde{y}$, $\tilde{z}$ non-

---

* *Definitions of terms are given in LIST OF SYMBOLS Section.*

9. *N. Gerber, R. Sedney, and J.M. Bartos, "Pressure Moment on a Liquid-Filled Projectile: Solid Body Rotation," ARBRL-TR-02422, October 1982. (ADA 120567).*

10. *C.H. Murphy, "Angular Motion of a Spinning Projectile With a Viscous Liquid Payload," BRL Memorandum Report ARBRL-MR-3194, July 1982. AD A118676.*

11. *W.P. D'Amico, Jr., and T.H. Rogers, "Yaw Instabilities Produced by Rapidly Rotating, Highly Viscous Liquids," AIAA Paper 81-0224, AIAA 19th Aerospace Sciences Meeting, St. Louis, Missouri, 12-15 January 1981.*

12. *R. Whiting and N. Gerber, "Dynamics of a Liquid-Filled Gyroscope: Update of Theory and Experiment," BRL Technical Report ARBRL-TR-02221, March 1980. AD A083886.*

rolling system which has the $\tilde{x}$-axis along the projectile axis of symmetry and the $\tilde{z}$-axis initially in the vertical plane. These systems are shown in Figure 1; the $\tilde{y}$ and $\tilde{z}$ axes are omitted for clarity.

The $x = 0$ and $\tilde{x} = 0$ values are located at the midplanes of the unyawed and yawed cylinders, respectively. The $\tilde{x}$-axis is nutating about the x-axis at the angle $K_1 = K_1(t)$. The components of the projection in the y, z plane of a unit vector lying on the $\tilde{x}$-axis are denoted by n_{YE} and n_{ZE}.

The yawing motion is characterized by two variables, $\tilde{\alpha}$ and $\tilde{\beta}$. The angle of attack, $\tilde{\alpha}$, in the aeroballistic system is the angle in the vertical plane measured from the $\tilde{x}$-axis to the velocity vector; the angle of sideslip, $\tilde{\beta}$, is the angle in the horizontal plane measured also from the $\tilde{x}$-axis to the velocity vector. For the small yaw angles considered, $\tilde{\alpha} \simeq -n_{ZE}$ and $\tilde{\beta} \simeq -n_{YE}$. It is convenient to combine $\tilde{\alpha}$ and $\tilde{\beta}$ into a single complex variable:

$$\tilde{\xi} \equiv \tilde{\beta} + i\,\tilde{\alpha} \simeq -(n_{YE} + i\,n_{ZE}) \tag{2.1}$$

The fluid pressure and viscous forces on the cavity surfaces produced by the motion give rise to a moment on the projectile. The spin-decelerating component, $M_{L\tilde{X}}$, is zero to the approximation considered here; the other components can be represented in complex form, $M_{L\tilde{Y}} + iM_{L\tilde{Z}}$. We shall consider only the liquid moment acting on the projectile; the liquid moment can be added to the other moments acting on shell or gyroscope as required. The differential equation of yawing motion is*

$$I_y\, d^2\tilde{\xi}/dt^2 - i\dot{\phi}\, I_x\, d\tilde{\xi}/dt + I_y\, \hat{M}\, \tilde{\xi} = i\,(M_{L\tilde{Y}} + iM_{L\tilde{Z}}). \tag{2.2}$$

The quantity I_x is the moment of inertia of the empty axisymmetric shell about its longitudinal axis. I_y is the transverse moment of inertia of the empty shell about its center of gravity. The spin rate of the shell is $\dot{\phi}$, which is taken to be positive in this work, and t is time. The term $I_y\, \hat{M}\, \tilde{\xi}$ is an aerodynamic moment for a projectile. For a gyroscope this term is a gravitational moment arising from the separation of center of gravity and pivot point, and in most experiments is zero.

---

* *This is Eq. (2.4) of Reference 10 with only the liquid moment on the right-hand side.*

In general there is an interaction between the motion of the projectile and the liquid motion. Here we shall specify the motion of the projectile. In particular the cylinder is nutating with constant frequency and exponentially-growing yaw:

$$\tilde{\xi} = (K_o e^{\varepsilon\tau\dot{\phi}t}) e^{i(\tau\dot{\phi}t)} = K_1 e^{i\phi_1} = K_o e^{if\dot{\phi}t}, \tag{2.3}$$

where

$$K_1 \equiv K_o e^{\varepsilon\tau\dot{\phi}t}, \quad \phi_1 \equiv \tau\dot{\phi}t, \quad f \equiv (1-i\varepsilon)\tau. \tag{2.4}$$

Here K_o is the magnitude of the yaw at time $t = 0$, τ is the nutational frequency divided by $\dot{\phi}$, and ε is a yaw growth rate or decay per nutational cycle. Also K_1 is the yaw amplitude, and ϕ_1 is the angular orientation* of the $\tilde{x}$-axis in the x, y, z system as shown in Figure 1.

The motion of the projectile enters the flow problem via the boundary conditions. Under the assumption that the flow is in phase with the motion of the shell, the pressure disturbance will have the time dependence of Eq. (2.3), and consequently the liquid moment will also have this form. A nondimensional liquid moment coefficient, C_{LM}, is now defined:**

$$M_{L\tilde{Y}} + i\, M_{L\tilde{Z}} = m_L\, a^2 \dot{\phi}^2\, \tau\, C_{LM}\, K_1 e^{i\phi_1}, \tag{2.5}$$

where m_L is the mass of the liquid and a is the radius of the cylinder cross-section. C_{LM} is a complex quantity whose real part represents a moment that changes the yaw angle, and whose imaginary part represents a moment that changes the nutation rate. Thus:

$$C_{LM} \equiv C_{LSM} + i\, C_{LIM}, \tag{2.6}$$

where C_{LSM} and C_{LIM} represent the "liquid side moment" and "liquid in-plane moment," respectively. As in Reference 9, we shall concentrate our attention on C_{LSM}, the liquid side moment.

---

* *For simplicity the angle of attack is assumed to be initially zero and the angle of sideslip to be initially positive; i.e., ϕ_{10} of Reference 10 is zero.*

** *See Eq. (2.7) in Reference 10.*

When the forcing moment in Eq. (2.5), produced by the motion specified in Eq. (2.3), is inserted into the yaw equation, Eq. (2.2), it is seen that the $\tilde{\xi}$ of Eq. (2.3) is a solution to Eq. (2.2) for a restricted set of f's, namely those satisfying the functional equation

$$I_y f^2 - I_x f - I_y \hat{M}/\dot{\phi}^2 = -i\,(2\pi\rho a^4 c)\,\tau\, C_{LM}\,(f;\ Re,\ c/a). \tag{2.7}$$

Here c is the half-height of the cylinder, ρ is the density of the liquid, and Re is Reynolds number defined by

$$Re = a^2\dot{\phi}/\nu, \tag{2.8}$$

where ν is kinematic viscosity of the liquid.

According to the Stewartson-Wedemeyer theory[4,6], C_{LM} of Eq. (2.7) is negligibly small except near resonance. A resonance condition will generally occur when $\tau_n \approx C_R$, where $\tau_n\,\dot{\phi}$ is the nutational frequency of the empty shell and $C_R\,\dot{\phi}$ is a natural inertial frequency of the rotating liquid.

$$\tau_n = \left[I_x + \left(I_x^2 + 4\,I_y\,\hat{M}/\dot{\phi}^2\right)^{1/2}\right] \Big/ (2\,I_y). \tag{2.9}$$

For $\tau \approx C_R$, C_{LM} can be approximated by the first term of the Laurent series of a function with a simple pole[4,6]

$$C_{LM} \cong \bar{D}/(f - C_R),$$

where the residue, $\bar{D}$, depends on the parameters of the problem.

III. COORDINATE AND VELOCITY TRANSFORMATIONS

The flow problem is stated and solved in terms of the inertial cylindrical coordinates x, r, θ (where $y = r\cos\theta$, $z = r\sin\theta$). However, the pressure and viscous forces are integrated over constant $\tilde{x}$ and $\tilde{r}$ surfaces to obtain moments (where $\tilde{y} = \tilde{r}\cos\tilde{\theta}$, $\tilde{z} = \tilde{r}\sin\tilde{\theta}$). Also, the original statement of boundary conditions is made in terms of $\tilde{x}$, $\tilde{r}$, $\tilde{\theta}$ coordinates. Thus, it is useful to have the tranformations between the two coordinate systems. From Eq. (9) of Reference 9, applicable for small K_o,

$$\left.\begin{aligned} r &= \tilde{r} - K_1\ (\tilde{x} - \ell)\cos(\phi_1 - \tilde{\theta}) + O(K_o^2) \\ \theta &= \tilde{\theta} - K_1\,[(\tilde{x} - \ell)/\tilde{r}]\sin(\phi_1 - \tilde{\theta}) + O(K_o^2) \\ x &= \tilde{x} + K_1\,\tilde{r}\cos(\phi_1 - \tilde{\theta}) + O(K_o^2), \end{aligned}\right\} \tag{3.1}$$

where ℓ is the x (and $\tilde{x}$) coordinate of the pivot point. All the above terms are nondimensional; lengths and distances are nondimensionalized by a. The transformation may also be expressed as

$$\left.\begin{aligned} \tilde{y} &= r\cos\theta + (K_1\cos\phi_1)(x-\ell) \\ \tilde{z} &= r\sin\theta + (K_1\sin\phi_1)(x-\ell) \\ \tilde{x} &= x - K_1 r\cos(\phi_1-\theta). \end{aligned}\right\} \qquad (3.2)$$

We define the flow to be a small disturbance to a basic flow, which is taken to be solid-body rotation in an unyawed cylinder. The Navier-Stokes equations are linearized to produce the perturbation equations.* The flow variables are the radial, azimuthal, and axial velocity components, and pressure, given here in nondimensional form:

$$u_{NS} = U - K_o\overset{*}{u}, \quad v_{NS} = V - K_o\overset{*}{v}, \quad w_{NS} = W - K_o\overset{*}{w}, \quad p_{NS} = P - K_o\overset{*}{p}. \qquad (3.3)$$

The symbols u_{NS}, v_{NS}, w_{NS}, and p_{NS} represent the total values, solutions of the linearized Navier-Stokes equations. U, V, W, and P are the basic undisturbed variables; and $\overset{*}{u}$, $\overset{*}{v}$, $\overset{*}{w}$, and $\overset{*}{p}$ are perturbation variables** of order one.*** For solid-body rotation, the basic flow is

$$U = 0, \quad V = r, \quad W = 0, \quad P = (1/2)r^2 + \text{const.} \qquad (3.4)$$

The velocity components are nondimensionalized by $a\dot{\phi}$, and pressure by $\rho a^2\dot{\phi}^2$.

In the aeroballistic system, the radial, azimuthal, and axial velocity perturbation components are denoted by $\overset{*}{\tilde{u}}$, $\overset{*}{\tilde{v}}$, and $\overset{*}{\tilde{w}}$. The velocity transformation, from Eq. (A.2) of Reference 9, is given by

---

* *These are Eq. (3) in Reference 3.*

** *The negative signs in Eq. (3.3) were employed to comply with the nomenclature of Reference 10.*

*** *The symbols u_{NS}, v_{NS}, w_{NS}, p_{NS} replace the symbols u, v, w, p in Eq. (10) of Reference 9.*

$$
\left.
\begin{aligned}
\overset{*}{u} &= \overset{*}{\tilde{u}} - (\tilde{x}-\ell)e^{\varepsilon\tau\dot{\phi}t}[\varepsilon\tau\cos(\phi_1-\tilde{\theta}) + (1-\tau)\sin(\phi_1-\tilde{\theta})] + O(K_o) \\
\overset{*}{v} &= \overset{*}{\tilde{v}} - (\tilde{x}-\ell)e^{\varepsilon\tau\dot{\phi}t}[-(1-\tau)\cos(\phi_1-\tilde{\theta}) + \varepsilon\tau\sin(\phi_1-\tilde{\theta})] + O(K_o) \\
\overset{*}{w} &= \overset{*}{\tilde{w}} - \tilde{r}\,e^{\varepsilon\tau\dot{\phi}t}[-\varepsilon\tau\cos(\phi_1-\tilde{\theta}) - (1-\tau)\sin(\phi_1-\tilde{\theta})] + O(K_o).
\end{aligned}
\right\} \qquad (3.5)
$$

The tilde superscripts can be dropped from the second terms of the right-hand sides of Eq. (3.1) and (3.5) without changing the order of error.

IV. FLOW SOLUTION AND WALL FORCES

A. Flow Solution

Chapter III of Reference 9 treats the flow problem in detail; we extract from it what is needed here. The flow variables are shown in Eqs. (3.3) and (3.4); the perturbed flow solution is

$$
\left.
\begin{aligned}
\overset{*}{u} &= \text{Real}\,[\underline{u}(r,x)\exp\{i(f\dot{\phi}t-\theta)\}] \\
\overset{*}{v} &= \text{Real}\,[\underline{v}(r,x)\exp\{i(f\dot{\phi}t-\theta)\}] \\
\overset{*}{w} &= \text{Real}\,[\underline{w}(r,x)\exp\{i(f\dot{\phi}t-\theta)\}] \\
\overset{*}{p} &= \text{Real}\,[\underline{p}(r,x)\exp\{i(f\dot{\phi}t-\theta)\}]
\end{aligned}
\right\} \qquad (4.1)
$$

where $\underline{u}$, $\underline{v}$, $\underline{w}$, and $\underline{p}$ are complex functions. These are expressed as the sums of two solutions:

$$
\left.
\begin{aligned}
\underline{u} &\equiv \underline{u}_R + i\,\underline{u}_I = \underline{u}_p + \underline{u}_H, & \underline{v} &\equiv \underline{v}_R + i\,\underline{v}_I = \underline{v}_p + \underline{v}_H \\
\underline{w} &\equiv \underline{w}_R + i\,\underline{w}_I = \underline{w}_p + \underline{w}_H, & \underline{p} &\equiv \underline{p}_R + i\,\underline{p}_I = \underline{p}_p + \underline{p}_H,
\end{aligned}
\right\} \qquad (4.2)
$$

where

$$
\left.
\begin{aligned}
\underline{u}_p &= -i[(1-f)^2/(1+f)]x + i(1-f)\ell, & \underline{v}_p &= -[(1-f)^2/(1+f)]x + (1-f)\ell \\
\underline{w}_p &= i(1-f)r, & \underline{p}_p &= -(1-f)^2 rx + (1-f^2)\ell r
\end{aligned}
\right\} \qquad (4.3)
$$

is a particular solution. The sub-H quantities are solutions of the following equations, where subscripts denote partial differentiation and the sub-H is omitted for clarity:

$$\left.\begin{aligned} & r\underline{u}_r + \underline{u} - i\underline{v} + r\underline{w}_x = 0 \\ & i(f-1)\underline{u} - 2\underline{v} = -\underline{p}_r + (1/Re)[\underline{u}_{rr} + \underline{u}_r/r - 2\underline{u}/r^2 + \underline{u}_{xx} + 2i\underline{v}/r^2] \\ & i(f-1)\underline{v} + 2\underline{u} = i\underline{p}/r + (1/Re)[\underline{v}_{rr} + \underline{v}_r/r - 2\underline{v}/r^2 + \underline{v}_{xx} - 2i\underline{u}/r^2] \\ & i(f-1)\underline{w} = -\underline{p}_{-x} + (1/Re)[\underline{w}_{rr} + \underline{w}_r/r - \underline{w}/r^2 + \underline{w}_{xx}]. \end{aligned}\right\} \quad (4.4)$$

These quantities further satisfy the boundary conditions at the sidewall

$$\left.\begin{aligned} & \underline{u}_H\,(r=1) = -i[2f(1-f)/(1+f)]x \\ & \underline{v}_H\,(r=1) = -[2f(1-f)/(1+f)]x \\ & \underline{w}_H\,(r=1) = 0, \end{aligned}\right\} \quad (4.5)$$

and at the endwall (where $\bar{\bar{c}} \equiv c/a$)

$$\underline{u}_H\,(x=\bar{\bar{c}}) = -i[2f(1-f)/(1+f)]\bar{\bar{c}}, \qquad \underline{u}_H\,(x=-\bar{\bar{c}}) = -\underline{u}_H\,(x=\bar{\bar{c}}) \quad (4.6a)$$

$$\underline{v}_H\,(x=\bar{\bar{c}}) = -[2f(1-f)/(1+f)]\bar{\bar{c}}, \qquad \underline{v}_H\,(x=-\bar{\bar{c}}) = -\underline{v}_H\,(x=\bar{\bar{c}}) \quad (4.6b)$$

$$\underline{w}_H\,(x=\bar{\bar{c}}) = \underline{w}_H\,(x=-\bar{\bar{c}}) = 0, \quad (4.6c)$$

plus boundary conditions at $r = 0$.

As explained in Reference 9, a modal solution (separation of variables) is required, but it cannot satisfy Eqs. (4.6a) and (4.6b). The need to drop two of the three endwall conditions implies that we have a singular perturbation problem; i.e., we must insert a boundary-layer or "inner" solution to satisfy these. The technique of matched asymptotic expansions is used to treat this problem. The solution $\underset{\sim}{u}_H$, $\underset{\sim}{v}_H$, etc., is decomposed into an outer solution, valid away from the endwall, and an inner solution, valid near the endwall. The expansions for each are determined to certain orders in the small parameter $Re^{-1/2}$ and a composite solution is formed. The velocity gradients at the endwall needed for the shear force are obtained from the composite solution.

In Reference 10 the viscous correction of Wedemeyer,[b] originally used to correct eigenvalues, is applied to correct velocities and pressure. Although the formalism of matched asymptotic expansions is not used there, the basic idea of obtaining a corrected flow is carried out. It is called the "inviscid flow" in Reference 10 even though it depends on Re; it would correspond to what is called outer flow here.

The outer solution, designated by u, v, w, p, satisfies Eqs. (4.4), (4.5), and (4.6c). The modal form of the outer solution is

$$\left.\begin{aligned} u &= \sum_{k=1} \hat{u}_k(r) \sin \lambda_k x, \qquad v = \sum_{k=1} \hat{v}_k(r) \sin \lambda_k x \\ w &= -\sum_{k=1} \hat{w}_k(r) \cos \lambda_k x, \qquad p = \sum_{k=1} \hat{p}(r) \sin \lambda_k x, \end{aligned}\right\} \tag{4.7}$$

where $\hat{u}_k$, $\hat{v}_k$, $\hat{w}_k$, and $\hat{p}_k$ are complex functions of r; they are solutions to the ordinary differential equations, Eqs. (33), with boundary conditions, Eqs. (37) and (41), of Reference 9. This is the usual normal mode solution with $\lambda_k = k\pi/2\bar{\bar{c}}$, where k is an odd integer. In Reference 9 it is shown that the outer solution is determined by the single condition of no flow through the endwall, Eq. (4.6c), to the order $0(Re^{-1/2})$; Eqs. (4.6a) and (4.6b) are not used or satisfied. The accuracy of the solution to this order is unacceptable. To improve it, the second term of the outer solution must be obtained, which, in turn, requires the first term of the inner solution and appropriate matching of the outer and inner solutions. As shown in Reference 9, this process yields the one boundary condition

$$w \mp \delta w_x = 0 \qquad \text{at } x = \pm \bar{\bar{c}} \tag{4.8}$$

to the order $0\ (Re^{-1})$. (It has since been shown that this boundary condition is correct to $0\ (Re^{-3/2})$.) The form of the solution is still Eq. (4.7), but the λ_k are complex, determined from the eigenvalue relation

$$\cos \lambda_k \bar{\bar{c}} + \lambda_k \, \delta c \sin \lambda_k \bar{\bar{c}} = 0, \tag{4.9}$$

where δc is given by the following sequence:

$$\left.\begin{aligned} \alpha &= 2^{-1/2} Re^{1/2} (1-i)\ (3-f)^{1/2} \\ \beta &= 2^{-1/2} Re^{1/2} (1+i)\ (1+f)^{1/2} \\ \delta c &= \left[\frac{1}{2\alpha} \left(1 - \frac{2}{1-f} \right) + \frac{1}{2\beta} \left(1 + \frac{2}{1-f} \right) \right]. \end{aligned}\right\} \tag{4.10}$$

The complex square roots are chosen to be the ones that make the real parts of α and β positive. When $\delta c / \bar{\bar{c}} \ll 1$, λ_k can be approximated by

$$\lambda_k \cong (k\pi)/[2(\bar{\bar{c}} - \delta c)]. \qquad \underline{(k \text{ odd})}$$

The first term of the inner solution is determined by the boundary layer equations, the no-slip conditions on the endwall, and boundary conditions at the boundary-layer edge derived by matching. These are given in Reference 9, pages 53 and 54.

The theory of matched asymptotic expansions, MAE, is the proper technique for dealing with these problems; in order to explain the results for shear force given in this report the discussion of MAE in Reference 9 must be augmented. Usually MAE are used to obtain an analytic solution to a problem with, possibly, some numerical integration required; this can be done for the present problem, at least in principle. Of course, it becomes increasingly tedious to obtain higher order terms. Since the problem of Eqs. (4.4) - (4.6) is linear, application of MAE here is simpler than for many other cases to which it is applied. Advantages of MAE are the systematized approach to the terms in the expansions, the clear distinction between inner and outer solutions and the matching of these.

Here the formalism of MAE is used to (1) distinguish the outer solution, determined as above, (2) rationalize the use of only one boundary condition, Eq. (4.6c), rather than three at the endwall, and (3) derive Eq. (4.8). The solution, Eq. (4.7), with appropriate λ_k would be the exact outer solution (requiring only ordinary differential equations to be integrated numerically), except that Eq. (4.8) is not exact. In the final form of the solution, the

analytically determined outer flow is replaced by the solution of Eqs. (4.7) and (4.9). This step leads to more accurate results at low Re though, strictly speaking, it is not part of the theory.

The first term of the inner solution is given, in the notation of Appendix D, Reference 9, by

$$\left.\begin{aligned} u_i\ (y,r) &= u_o^o\ (\bar{\bar{c}},\ r) + (i/2)\ [Ae^{-\alpha y} - Be^{-\beta y}] \\ v_i\ (y,r) &= v_o^o\ (\bar{\bar{c}},\ r) - (1/2)\ [Ae^{-\beta y} + Be^{-\beta y}] \\ w_i\ (y,r) &= Re^{1/2}\ (\partial w_o^o/\partial x)_{x=\bar{\bar{c}}}\ \Big\{ \delta c - y + [(1+f)/2\alpha(1-f)]\ \exp\ (-\alpha y) - \\ &\qquad [(3-f)/2\beta(1-f)]\ \exp\ (-\beta y) \Big\}, \end{aligned}\right\} \quad (4.11)$$

where $y = \bar{\bar{c}} - x$

and

$$\left.\begin{aligned} A(r) &= v_o^o + iu_o^o \\ B(r) &= v_o^o - iu_o^o + 4f\ [(1-f)/(1+f)]\ \bar{\bar{c}} \end{aligned}\right\} \quad \text{at } x = \bar{\bar{c}}. \quad (4.12)$$

The functions u_o^o, v_o^o, and w_o^o are defined in Reference 9, page 53. The expressions for u_i and v_i in Eq. (4.11) would be the same as the boundary-layer solutions of Wedemeyer[6] if the inviscid terms in the latter were evaluated at the endwall.

From the inner and outer expansions a single expansion, uniformly valid in the inner and outer regions, can be constructed; it is called the composite expansion. Using a 1-term inner and a 2-term outer expansion, the composite expansions are:

$$\left.\begin{aligned} u_C &= u_o^o\ (\bar{\bar{c}}-y,r) + Re^{-1/2}\ u_{o1}^o\ (\bar{\bar{c}}-y,r) + (i/2)\ [Ae^{-\alpha y} - Be^{-\beta y}] \\ v_C &= v_o^o\ (\bar{\bar{c}}-y,r) + Re^{-1/2}\ v_{o1}^o\ (\bar{\bar{c}}-y,r) - (1/2)\ [Ae^{-\alpha y} + Be^{-\beta y}] \\ w_C &= w_o^o\ (\bar{\bar{c}}-y,r) + Re^{-1/2}\ w_{o1}^o\ (\bar{\bar{c}}-y,r), \end{aligned}\right\} \quad (4.13)$$

where the functions u_{01}^{o}, v_{01}^{o}, w_{01}^{o} are defined in Reference 9, page 53. The gradients of u_C and v_C, $(\partial/\partial y)_{y=0} = -(\partial/\partial x)_{x=\bar{c}}$, are required to obtain the endwall shear. The matching process shows that $\left[(\partial/\partial x)_{x=\bar{c}}\right]$ of u_o^o, u_{01}^o, v_o^o, v_{01}^o are all zero. Therefore,

$$\left.\begin{aligned}(\partial u_C/\partial y)_{y=0} &= -(i/2)\,[\alpha A - \beta B]\\ (\partial v_C/\partial y)_{y=0} &= (1/2)\,[\alpha A + \beta B]\end{aligned}\right\} \qquad (4.14)$$

Thus, these gradients at the endwall could be computed from just the inner solution.

At the sidewall, the no-slip boundary conditions are satisfied by the solution to Eqs. (4.4) and (4.5). The necessary gradients at the sidewall are obtained directly from the modal solution.

B. Shear Forces

Forces on the surface of the cylinder are obtained from the 3×3 stress tensor, which gives the force on the fluid. (See, e.g., Reference 13, page 53, where z is axial coordinate.) Since we want the force on the cylinder, the sign of the stress tensor is changed from that of Reference 13. The elements of the tensor are

$$\tau_{rr} = P - K_o\,[\overset{*}{p} - (2/Re)\,\partial\overset{*}{u}/\partial r] \qquad (4.15a)$$

$$\tau_{\theta\theta} = P - K_o\,[\overset{*}{p} - 2\,(\overset{*}{u} + \partial\overset{*}{v}/\partial\theta)/(Re\ r)] \qquad (4.15b)$$

$$\tau_{xx} = P - K_o\,[\overset{*}{p} - (2/Re)\,(\partial\overset{*}{w}/\partial x)] \qquad (4.15c)$$

$$\tau_{r\theta} = \tau_{\theta r} = (K_o/Re)\,[r\,\partial(\overset{*}{v}/r)/\partial r + (\partial\overset{*}{u}/\partial\theta)/r] \qquad (4.15d)$$

$$\tau_{rx} = \tau_{xr} = (K_o/Re)\,[\partial\overset{*}{u}/\partial x + \partial\overset{*}{w}/\partial r] \qquad (4.15e)$$

$$\tau_{\theta x} = \tau_{x\theta} = (K_o/Re)\,[\partial\overset{*}{v}/\partial x + (1/r)\,\partial\overset{*}{w}/\partial\theta] \qquad (4.15f)$$

---

13. H. Schlichting, Boundary Layer Theory, McGraw-Hill Book Co., New York, NY, 1960.

The nondimensional force on an element of the cylinder surface with nondimensional area dA will be denoted by

$$dF = (dF_r,\ dF_\theta,\ dF_x), \tag{4.16}$$

where dF_r, dF_θ, dF_x are the force components in the radial, azimuthal, and axial directions, respectively, in the earth-fixed frame. Force is nondimensionalized by $\rho a^4 \dot{\varphi}^2$, where ρ is density of the liquid, and area is nondimensionalized by a^2. Then

$$dF_r = (\tau_{rr}\, g_r + \tau_{r\theta}\, g_\theta + \tau_{rx}\, g_x)\, dA \tag{4.17a}$$

$$dF_\theta = (\tau_{\theta r}\, g_r + \tau_{\theta\theta}\, g_\theta + \tau_{\theta x}\, g_x)\, dA \tag{4.17b}$$

$$dF_x = (\tau_{xr}\, g_r + \tau_{x\theta}\, g_\theta + \tau_{xx}\, g_x)\, dA, \tag{4.17c}$$

where g_r, g_θ, g_x are the radial, azimuthal, and axial components in the inertial frame of a unit vector (directed outward from the container; i.e., away from the fluid) normal to the element of wall surface. If the surface is given in the form $G(r, \theta, x) = \text{const}$, then

$$g_r = \frac{\partial G/\partial r}{|\nabla G|}, \qquad g_\theta = \frac{(1/r)\,\partial G/\partial \theta}{|\nabla G|}, \qquad g_x = \frac{\partial G/\partial x}{|\nabla G|}, \tag{4.18}$$

where $|\nabla G| \equiv + \left[(\partial G/\partial r)^2 + (1/r^2)\,(\partial G/\partial \theta)^2 + (\partial G/\partial x)^2\right]^{1/2}$

At the sidewall, $\tilde{r}(r, \theta, x) = 1$, and at the endwalls, $\tilde{x}(r, \theta, x) = \pm \bar{\tilde{c}}$. From Eqs. (3.1) and (3.2) we obtain unit normals, $N = (g_r, g_\theta, g_x)$ to sidewall and endwall, accurate to order K_0:

$$N_{side} = (1, \quad K_1\,[(x-\ell)/r]\sin[\phi_1-\theta], \quad K_1 \cos[\phi_1-\theta]) \tag{4.19a}$$

$$N_{top} = (-K_1 \cos[\phi_1-\theta], \quad -K_1 \sin[\phi_1-\theta], \quad 1) \tag{4.19b}$$

$$N_{bottom} = -N_{top} \tag{4.19c}$$

The nondimensional surface element areas are

$$dA_{\tilde{r}=1} = d\tilde{\theta}\, d\tilde{x}, \qquad dA_{\tilde{x}=\pm\bar{\tilde{c}}} = \tilde{r}\, d\tilde{r}\, d\tilde{\theta}. \tag{4.20}$$

Combining Eqs. (4.15), (4.17), (4.19), and (4.20), we obtain the surface forces correct to order K_0.

At the sidewall ($\tilde{r} = 1$)

$$\left.\begin{aligned} dF_r/(d\tilde{\theta}\, d\tilde{x}) &= P - K_o \left[\overset{*}{p} - (2/Re)\, \partial \overset{*}{u}/\partial r\right] \\ \frac{dF_\theta}{d\tilde{\theta}\, d\tilde{x}} &= \frac{K_o}{Re}\left[r \frac{\partial}{\partial r}\frac{\overset{*}{v}}{r} + \frac{1}{r}\frac{\partial \overset{*}{u}}{\partial \theta}\right] + K_1 P \frac{x-\ell}{r} \sin(\phi_1 - \theta) \\ dF_x/(d\tilde{\theta}\, d\tilde{x}) &= (K_o/Re)\left[\partial \overset{*}{u}/\partial x + \partial \overset{*}{w}/\partial r\right] + K_1 P \cos(\phi_1 - \theta). \end{aligned}\right\} \quad (4.21)$$

At the top wall ($\tilde{x} = \bar{\tilde{c}}$)

$$\left.\begin{aligned} dF_r/(\tilde{r}\, d\tilde{r}\, d\tilde{\theta}) &= -K_1 P \cos(\phi_1 - \theta) + (K_o/Re)\left[\partial \overset{*}{u}/\partial x + \partial \overset{*}{w}/\partial r\right] \\ dF_\theta/(\tilde{r}\, d\tilde{r}\, d\tilde{\theta}) &= -K_1 P \sin(\phi_1 - \theta) + (K_o/Re)\left[\partial \overset{*}{v}/\partial x + (\partial \overset{*}{w}/\partial \theta)/r\right] \\ dF_x/(\tilde{r}\, d\tilde{r}\, d\tilde{\theta}) &= P - K_o \left[\overset{*}{p} - (2/Re)\, \partial \overset{*}{w}/\partial x\right]. \end{aligned}\right\} \quad (4.22)$$

At this point we introduce the boundary-layer assumptions, namely, that the tangential gradients of the velocity components at a surface are negligible, and that the normal gradient of the normal component is also negligible. The orders of magnitude of the velocity gradients at $x = \bar{\tilde{c}}$ in Eq. (4.22) can be determined explicitly from the MAE results, Eq. (4.13), and results of the matching:

$$\partial \overset{*}{u}/\partial x = O(Re^{1/2}) \qquad \partial \overset{*}{w}/\partial r = O(Re^{-1/2})$$

$$\partial \overset{*}{v}/\partial x = O(Re^{1/2}) \qquad \partial \overset{*}{w}/\partial \theta = O(Re^{-1/2})$$

$$\partial \overset{*}{w}/\partial x = O(1).$$

This approximation is not necessary for the further development of the theory; it is made here for convenience. It does restrict the applicability of the moment calculations to high (as yet undefined) Reynolds numbers. However, all the terms in the stress tensor are available from the solution to the flow problem; their contribution to the moment may be significant at low Reynolds numbers. Actually, a restriction to high Reynolds numbers has already been introduced by the boundary condition, Eq. (4.8).

Equations (4.21) and (4.22) reduce to

$$dF_r/(d\tilde{\theta}\, d\tilde{x}) = P - K_0 \overset{*}{p} \tag{4.23a}$$

$$dF_\theta/(d\tilde{\theta}\, d\tilde{x}) = (K_0/Re)\left[r\, \partial(\overset{*}{v}/r)/\partial r\right] + K_1 P \left[(x-\ell)/r\right] \sin(\phi_1-\theta) \tag{4.23b}$$

$$dF_x/(d\tilde{\theta}\, d\tilde{x}) = (K_0/Re)\, \partial \overset{*}{w}/\partial r + K_1 P \cos(\phi_1-\theta) \tag{4.23c}$$

at the sidewall, and

$$dF_r/(\tilde{r}\, d\tilde{r}\, d\tilde{\theta}) = -K_1 P \cos(\phi_1-\theta) + (K_0/Re)\, \partial \overset{*}{u}/\partial x \tag{4.24a}$$

$$dF_\theta/(\tilde{r}\, d\tilde{r}\, d\tilde{\theta}) = -K_1 P \sin(\phi_1-\theta) + (K_0/Re)\, \partial \overset{*}{v}/\partial x \tag{4.24b}$$

$$dF_x/(\tilde{r}\, d\tilde{r}\, d\tilde{\theta}) = P - K_0 \overset{*}{p} \tag{4.24c}$$

at the top wall. The expressions for force components on the bottom wall are the negatives of those for the components at the top wall, and $-\bar{\bar{c}}$ replaces $\bar{\bar{c}}$.

V. EVALUATION OF LIQUID MOMENT

A. Expression for Liquid Moment

We wish to determine the moment produced by the liquid on the spinning and nutating shell, namely, $M_{L\tilde{Y}} + i\, M_{L\tilde{Z}}$ of Eq. (2.5). We shall evaluate the moment about the center of gravity of the projectile in the $\tilde{x}$, $\tilde{y}$, $\tilde{z}$ system. Details need be shown for only one component, say $M_{L\tilde{Z}}$, since the form of Eq. (2.5) indicates that both $M_{L\tilde{Y}}$ and $M_{L\tilde{Z}}$ are determined by C_{LSM} and C_{LIM} of Eq. (2.6). In rectangular coordinates, the moment on an element of wall surface is the vector product of (1) the radius vector relative to pivot point $(\tilde{x}-\ell, \tilde{y}, \tilde{z})$ and (2) the force $dF = (dF_{\tilde{x}}, dF_{\tilde{y}}, dF_{\tilde{z}})$. The particular component that we treat is $M_{L\tilde{Z}}$:

$$dM_{L\tilde{Z}} = \rho a^5 \dot{\phi}^2 \left[(\tilde{x}-\ell)\, dF_{\tilde{y}} - \tilde{y}\, dF_{\tilde{x}}\right], \tag{5.1}$$

where $dF_{\tilde{x}}$ and $dF_{\tilde{y}}$ are the components of dF in the $\tilde{x}$ and $\tilde{y}$ directions, respectively. Unit vectors in the $\tilde{x}$ and $\tilde{y}$ directions are found by taking the normalized gradients of $\tilde{x}$ = const. and $\tilde{y}$ = const. of Eq. (3.2) in the manner

of Eq. (4.18); the scalar products of these unit vectors with dF of Eq. (4.16) yield the two force components

$$dF_{\tilde{y}} = dF_r \cos\theta - dF_\theta \sin\theta + dF_x K_1 \cos\phi_1 + 0\,(K_0^2) \tag{5.2a}$$

$$dF_{\tilde{x}} = -dF_r K_1 \cos(\phi_1-\theta) - dF_\theta K_1 \sin(\phi_1-\theta) + dF_x + 0\,(K_0^2) \tag{5.2b}$$

B. Sidewall Moment

The element of moment, $dM_{L\tilde{Z}}$, in Eq. (5.1) is evaluated at $\tilde{r} = 1$, and will be denoted by $dM_{L\tilde{Z}L}$. By Eqs. (3.4) and (3.1),

$$P\,(\tilde{r}=1) = \text{const.} - K_1 (\tilde{x}-\ell)\cos(\phi_1-\tilde{\theta}) + 0\,(K_0^2). \tag{5.3}$$

Application of Eqs. (4.23) and (5.2), yields

$$\frac{dF_{\tilde{y}}}{d\tilde{\theta}\,d\tilde{x}} = (P-K_0\overset{*}{p})\cos\theta - \left[\frac{K_0}{Re}\, r\,\frac{\partial}{\partial r}\frac{\overset{*}{v}}{r} + K_1 P\,\frac{(x-\ell)}{r}\sin(\phi_1-\theta)\right]\sin\theta + 0\,(K_0^2) \tag{5.4}$$

$$dF_{\tilde{x}}/(d\tilde{\theta}\,d\tilde{x}) = (K_0/Re)\,\partial\overset{*}{w}/\partial r + 0\,(K_0^2)$$

We apply Eqs. (5.3) and (5.4) and integrate Eq. (5.1) at $\tilde{r} = 1$, noting that the constant part of P makes no contribution to the integral, leaving only first order terms in K_0. Thus, the variables $\tilde{r}$, $\tilde{\theta}$, $\tilde{x}$ may be replaced by r, θ, x and the integral evaluated at $r = 1$ without changing the first order accuracy. Integration yields

$$M_{L\tilde{Z}L}/(K_0 \rho a^5 \dot{\phi}^2) = -\int_{-\bar{c}}^{\bar{c}}\int_0^{2\pi}\left[(x-\ell)\left\{\overset{*}{p} + e^{\varepsilon\tau}\dot{\phi}t\,(x-\ell)\cos(\phi_1-\theta)\right\} + (\partial\overset{*}{w}/\partial r)/Re\right]\cos\theta\,d\theta\,dx \; - \tag{5.5}$$

$$(1/Re)\int_{-\bar{c}}^{\bar{c}}\int_0^{2\pi}\left[(x-\ell)\left\{\partial\overset{*}{v}/\partial r - \overset{*}{v}\right\}\right]\sin\theta\,d\theta\,dx + 0\,(K_0^2).$$

Further manipulations lead to the following formula, with application of Eqs. (2.5), (2.6), (4.1), and (4.2), plus the boundary condition $\underline{v}(r=1) = -(1-f) \times (x-\ell)$:

$$M_{L\tilde{Z}L}/(2\pi\rho a^4 c \dot{\phi}^2 \tau K_1) = C_{(LSM)PL} \sin \phi_1 + C_{(LIM)PL} \cos \phi_1 + C_{(LSM)VL} \sin \phi_1 + C_{(LIM)VL} \cos \phi_1, \tag{5.6}$$

where integrals are evaluated at r=1, and

$$C_{(LSM)PL} = (2\tau \bar{\bar{c}})^{-1} \int_{-\bar{\bar{c}}}^{\bar{\bar{c}}} (x-\ell)\, \underline{p}_I \, dx \tag{5.7a}$$

$$C_{(LIM)PL} = -(2\tau \bar{\bar{c}})^{-1} \int_{-\bar{\bar{c}}}^{\bar{\bar{c}}} (x-\ell) \left[\underline{p}_R + (x-\ell)\right] dx \tag{5.7b}$$

$$C_{(LSM)VL} = -\frac{1}{2\tau \bar{\bar{c}}\, Re} \int_{-\bar{\bar{c}}}^{\bar{\bar{c}}} \left\{ -\frac{\partial \underline{w}_I}{\partial r} + (x-\ell)\left[\frac{\partial \underline{v}_R}{\partial r} + (1-\tau)(x-\ell)\right]\right\} dx \tag{5.7c}$$

$$C_{(LIM)VL} = -\frac{1}{2\tau \bar{\bar{c}}\, Re} \int_{-\bar{\bar{c}}}^{\bar{\bar{c}}} \left\{ \frac{\partial \underline{w}_R}{\partial r} + (x-\ell)\left[\frac{\partial \underline{v}_I}{\partial r} + \varepsilon\tau (x-\ell)\right]\right\} dx. \tag{5.7d}$$

In the labeling of the moment coefficients of Eqs. (5.6) and (5.7), the LSM and LIM designations are defined in Chapter II (Eq. (2.5) et seq.), P indicates pressure, V indicates viscous wall shear, and the final L (lateral) designates sidewall.

C. Endwall Moment

The element of moment, $dM_{L\tilde{Z}}$, in Eq. (5.1), evaluated at $\tilde{x} = \bar{\bar{c}}$ and $\tilde{x} = -\bar{\bar{c}}$, will be denoted by $dM_{L\tilde{Z}T}$ and $dM_{L\tilde{Z}B}$, respectively. The element of total endwall moment is

$$dM_{L\tilde{Z}E} = dM_{L\tilde{Z}T} + dM_{L\tilde{Z}B}. \tag{5.8}$$

Application of Eqs. (4.24) and (5.2) yields

$$dF_{\tilde{y}}/(\tilde{r}\, d\tilde{r}\, d\tilde{\theta}) = (K_0/Re)\left[(\partial u^*/\partial x)\cos\tilde{\theta} - (\partial v^*/\partial x)\sin\tilde{\theta}\right] + O(K_0^2)$$

$$dF_{\tilde{x}}/(\tilde{r}\, d\tilde{r}\, d\tilde{\theta}) = P - K_0 p^* + O(K_0^2). \tag{5.9}$$

By Eqs. (3.4) and (3.1)

$$P(\tilde{x} = \bar{\tilde{c}}) = fn(\tilde{r}) - K_1 \tilde{r}(\bar{\tilde{c}} - \ell)\cos(\phi_1 - \tilde{\theta}) + O(K_0^2)$$

$$P(\tilde{x} = -\bar{\tilde{c}}) = fn(\tilde{r}) - K_1 \tilde{r}(-\bar{\tilde{c}} - \ell)\cos(\phi_1 - \tilde{\theta}) + O(K_0^2). \tag{5.10}$$

We obtain $dM_{L\tilde{Z}T}$ and $dM_{L\tilde{Z}B}$ separately using Eqs. (5.1), (5.9), and (5.10). The equations for the flow solution in Chapter IV show that $\partial u^*/\partial x$ and $\partial v^*/\partial x$ are even functions of x, leading to some cancellations when the top and bottom wall moments are added to produce

$$\frac{M_{L\tilde{Z}\tilde{R}}}{K_0 \rho a^5 \dot{\phi}^2} = \int_0^1 \int_0^{2\pi} \left[2\bar{\tilde{c}}\, e^{\varepsilon_1 \dot{\phi} t}\, \tilde{r}\cos(\phi_1 - \theta) + p^*(\bar{\tilde{c}}) - p^*(-\bar{\tilde{c}})\right] \tilde{r}^2 \cos\tilde{\theta}\, d\tilde{\theta}\, d\tilde{r} +$$

$$(2\bar{\tilde{c}}/Re) \int_0^1 \int_0^{2\pi} \left[(\partial u^*/\partial x)_{\bar{\tilde{c}}} \cos\theta - (\partial v^*/\partial x)_{\bar{\tilde{c}}} \sin\theta\right] \tilde{r}\, d\tilde{\theta}\, d\tilde{r}. \tag{5.11}$$

The $\tilde{r}$, $\tilde{\theta}$, $\tilde{x}$ may be replaced by r, θ, x in Eq. (5.11) and integrals evaluated at $x = \bar{\tilde{c}}$ without affecting the first order approximation in K_0.

Moment coefficients analogous to those for the sidewall will now be defined for the endwalls:

$$M_{L\tilde{Z}E}/(2\pi\rho a^4 \dot{\phi}^2 \tau K_1) = C_{(LSM)PE}\sin\phi_1 + C_{(LIM)PE}\cos\phi_1 +$$

$$C_{(LSM)VE}\sin\phi_1 + C_{(LIM)VE}\cos\phi_1, \tag{5.12}$$

where

$$C_{(LSM)PE} = -[1/(2\tau\bar{c})]\int_0^1 \left\{ \underline{p}_I(\bar{c}) - \underline{p}_I(-\bar{c}) \right\} r^2\, dr \tag{5.13a}$$

$$C_{(LIM)PE} = [1/(2\tau\bar{c})]\left[(\bar{c}/2) + \int_0^1 \left\{ \underline{p}_R(\bar{c}) - \underline{p}_R(-\bar{c}) \right\} r^2\, dr\right] \tag{5.13b}$$

$$C_{(LSM)VE} = -[1/(\tau\, Re)]\ \text{Real}\left[\int_0^1 \left\{ \partial(\underline{v}-i\underline{u})/\partial x \right\}_{\bar{c}} r\, dr\right] \tag{5.13c}$$

$$C_{(LIM)VE} = -[1/(\tau\, Re)]\ \text{Imag}\left[\int_0^1 \left\{ \partial(\underline{v}-i\underline{u})/\partial x \right\}_{\bar{c}} r\, dr\right]. \tag{5.13d}$$

The total side moment coefficients due to pressure and shear stress, respectively, are

$$\left.\begin{aligned} C_{(LSM)P} &= C_{(LSM)PL} + C_{(LSM)PE}, \\ C_{(LSM)V} &= C_{(LSM)VL} + C_{(LSM)VE}, \end{aligned}\right\} \tag{5.14}$$

and finally, the total side moment coefficient is

$$C_{LSM} = C_{(LSM)P} + C_{(LSM)V}. \tag{5.15}$$

The term $[\partial(\underline{v} - i\underline{u})/\partial x]_{x=\bar{c}}$ in Eq. (5.13) is evaluated from the complete solution, Eq. (4.2), $\underline{u} = \underline{u}_p + \underline{u}_H$ and $\underline{v} = \underline{v}_p + \underline{v}_H$. According to the method of solution described in Chapter IV, $\underline{u}_H$ and $\underline{v}_H$ are determined by the composite solutions u_C and v_C. Therefore, to the order of approximation in Eq. (5.13),

$$\underline{v} - i\underline{u} = \underline{v}_p - i\underline{u}_p + v_C - iu_C \tag{5.16}$$

$$= -2x(1-f)^2/(1+f) + 2\bar{\varepsilon}(1-f) + v_o^o - iu_o^o + Re^{-1/2}(v_{o1}^o - iu_{o1}^o) - Be^{-\eta y}$$

making use of Eqs. (4.3) and (4.13) and the definition of β in Eq. (4.10). The terms from the outer solution, including those in B, see Eq. (4.12), are not evaluated analytically; they are obtained from Eqs. (4.7) and (4.9), as explained in Chapter IV. Thus $\underline{v}-i\underline{u}$ can be written

$$\underline{v} - i\underline{u} = \underline{v}_p - i\underline{u}_p + v - iu - [(v - iu)_{x = \bar{\bar{c}}} + \left\{4f(1-f)/(1+f)\right\} \bar{\bar{c}}\ ]\, e^{-\beta y}. \tag{5.17}$$

Another useful form is obtained by expressing this in terms of $v + \underline{v}_p - i(u+\underline{u}_p)$:

$$\underline{v} - i\underline{u} = (v+\underline{v}_p) - i(u+\underline{u}_p) - [(v+\underline{v}_p)_{x = \bar{\bar{c}}} - i(u+\underline{u}_p)_{x = \bar{\bar{c}}} + 2(1-f)\ (\bar{\bar{c}} - \ell)]\, e^{-\beta y}. \tag{5.18}$$

The gradient term in Eqs. (5.13c) and (5.13d) is then

$$[\partial(\underline{v} - i\underline{u})/\partial x]_{x = \bar{\bar{c}}} = \left\{ \partial[(v+\underline{v}_p) - i(u+\underline{u}_p)]/\partial x \right\}_{x = \bar{\bar{c}}} - \beta[(v+\underline{v}_p)_{x = \bar{\bar{c}}} - i(u+\underline{u}_p)_{x = \bar{\bar{c}}} + 2(1-f)\ (\bar{\bar{c}} - \ell)]. \tag{5.19}$$

Empirically it is found that the first term on the right-hand side of Eq. (5.19) is small compared to the second term and is neglected when the gradient is evaluated; recall that $\beta = O(Re^{1/2})$. A strict estimate of the order of magnitude of these two terms in Eq. (5.19) is not straightforward because we have used u and v, obtained from Eq. (4.7), rather than the outer solutions. If the gradient is obtained from Eq. (5.16), the result is

$$[\partial\ (\underline{v}-i\underline{u})/\partial x]_{x=\bar{\bar{c}}} = -2(1-f)^2/(1+f) - \beta\ [v_o^o - iu_o^o + 4f(1-f)/(1+f)]_{x=\bar{\bar{c}}} \tag{5.20}$$

in which it is clear that the first term is O(1) and the second is $O(Re^{1/2})$. This result is reflected in the conclusion about the terms in Eq. (5.19) stated above.

VI. NUMERICAL RESULTS: MOMENT COEFFICIENT

A. Effect of Wall Shear

In Reference 10 it was shown that viscous shear could have a significant effect on the liquid moment at moderately high Reynolds numbers (~40,000). The pressure moments on sidewall and endwalls were opposed to each other in all computations performed ($C_{(LSM)P} > 0$ and $C_{(LSM)V} < 0$), while the shear moments on side and end walls were frequently of the same sign. Thus, the partial cancellation of the pressure moments and the reinforcement of the shear moments at times brought the two within the same order of magnitude.

Figures 2 and 3 illustrate the effect of viscous shear. At $\tau = 0.19$ and $Re = 4 \times 10^4$, e.g., the magnitude of shear moment is greater than 25% of pressure moment, certainly a nonnegligible contribution. The difference between $C_{(LSM)P}$ and C_{LSM} increases markedly as Re decreases. The qualitative behavior of side moment can also be affected by shear. Thus, at $\tau = 0.10$ in Figure 3, the pressure moment coefficient increases monotonically as Re decreases to 10^3, while the total moment coefficient peaks at $Re \approx 6300$ and changes sign at $Re \approx 2500$.

In Figure 2, $C_{(LSM)P}$ has a maximum near the eigenfrequency of the 2nd radial, 4th axial inertial mode (n=1, k=7) of the liquid as predicted by theory.[3] The magnitude of shear moment, $|C_{LSM)V}|$ also appears to have a maximum, though not as pronounced, in this region.

B. Comparison with Results of Murphy's Method

In Reference 10 Murphy solves the inviscid perturbation equations of Stewartson together with the viscous-corrected boundary conditions of Wedemeyer at sidewall and endwalls, and integrates the wall forces to obtain moments without assuming that the coning motion is nearly in resonance with inertial oscillations of the liquid. Comparisons between pressure moments obtained by Murphy's method and our method are given in Reference 9, where it is shown that agreement is good at very high Reynolds numbers but deteriorates with decreasing Reynolds number.

Figure 4 shows a comparison of the total moment coefficients for the case $c/a = 4.291$, $\varepsilon = 0$. For clarity the curves for $Re = 10^5$ and 10^6 have been omitted; the curves from the two methods are practically coincident on the scale of this figure. For $Re = 10^4$ agreement is still fairly good; but for $Re = 10^3$ the discrepancies are large, and for $Re = 10^2$ the two methods give C_{LSM}'s of opposite sign. There is no discernable peak in C_{LSM} for $Re = 10^3$ and 10^2 over the range of τ considered. The separate pressure and viscous moment coefficients for $Re = 10^5$ and 10^3 are shown plotted against τ in Figure 5. At $Re = 10^5$ the pairs of curves of the two theories are practically coincident; at $Re = 10^3$ and $\tau = 0.10$, the $C_{(LSM)P}$'s differ by 30% and the $C_{(LSM)V}$'s by a factor of 2.

C. Moments on Sidewall and Endwalls

Figures 6 and 7 illustrate the behavior of the separate components of the side moment coefficient for a cylinder of c/a = 3.126, executing motions of $\varepsilon = 0.02$ and $\tau = 0.020, 0.045$. When Reynolds number is varied by changing only ν, as in the experiments of Reference 14, the moment varies directly as the moment coefficient. It is seen then that pressure moments of both Murphy's and present theory vary nonmonotonically with Reynolds number, both on the sidewall and the endwalls. A major source of the difference between the results of the two theories lies in the methods of obtaining the outer flow, or, as designated in Reference 10, the "inviscid" flow (see p. 15, paragraph before Eq. (4.7)). The results in Figure 6 indicate that this difference is small; the location of the peak is a function of the nutational frequency.

In Figure 7 the variations of shear moments on the sidewall and endwalls are presented; they are not monotonic functions of Re and are negative in many instances so that they tend to damp yaw. From the natures of the present theory and that of Reference 10 the results from the two should approach each other for large Re. The results in Figure 7, and those for other values of τ, show that this occurs for $2\times10^4 \lesssim Re \lesssim 3.2\times10^5$ over the range $.02 \lesssim \tau \lesssim .045$. These are surprisingly large values of Re for an asymptotic approach of the results of the two theories. The differences in moment on the endwall, Figure 7b, are relatively small. The gradients there are obtained in the same way in both theories; however, the outer flows are different. The differences in moments on the sidewall, Figure 7a, are large for $Re \lesssim 10^4$. The methods of obtaining the gradients on the sidewall are quite different in the two theories. The only significant difference in the results from the two theories is found in Figure 7a. For the same Re and c/a, the yaw growth rate (shown in Figure 11) computed from the present theory agrees better with experimental data than that computed from Reference 10.

The variation of shear moment with Re on either the sidewall or endwall is not a simple power law. On the endwall, the shear moment would vary as $Re^{-1/2}$ if the analytically determined outer flow were used to obtain the gradient in Eq. (5.19), as explained in the discussion on Eqs. (5.19) and (5.20). The nonmonotonic variation shown in Figure 7b precludes such a variation; a power law variation would plot as negative exponential in Figure 7b. The same conclusion holds for the sidewall, Figure 7a, except that for $\tau = 0.020$ (and 0.030, not shown) the shear moment is monotonic with Re. However, if a power law fit, Re^{-n}, to the sidewall shear moment is tried, $0.55 \le n \le 0.81$ is obtained for $5\times10^3 \le Re \le 5\times10^5$. Note that in Reference 10, p. 34, it is stated that all shear moment coefficients vary as $Re^{-1/2}$. The results of Figure 7 show that this cannot be the case.

---

14. *W.P. D'Amico and M.C. Miller, "Flight Instability Produced by a Rapidly Spinning, Highly Viscous Liquid," Journal of Spacecraft and Rockets, Vol. 16, January-February 1979, pp. 62-64.*

VII. YAW GROWTH RATES: COMPARISON OF THEORY AND EXPERIMENT

Ultimately, the validity of the theory must be gauged by comparison of theoretical and experimental results. Measurements of nutational frequencies and yaw growth rates can be made in gyroscope experiments. The apparatus, operations, and accuracy of these experiments are discussed in References 11 and 12; they are thus far the only type of experiments available for comparison with the theory. The gyroscope can be used because the equation describing its oscillatory motion is analogous to that describing the yawing motion of a projectile. The relationship between gyroscope and projectile motions is discussed in Chapter 2 of Reference 2. The moments of inertia I_x and I_y in Eqs. (2.2) and (2.7) necessarily include parts of the apparatus. The term $I_y \hat{M} \tilde{\xi}$ in Eq. (2.2) is a gravitational moment arising from the separation of center of mass and pivot point. It will be zero here since these two positions are essentially coincident; thus ξ will be zero. The theoretical quantities, τ and ε, are obtained by solving Eq. (2.7) for $f \equiv (1-i\varepsilon)\tau$. The imaginary part of Eq. (2.7) can be written

$$\varepsilon\tau_n \left[1 + \left\{(\tau-\tau_n)/\tau_n)\right\}\right] \left[1 + \left\{(\tau-\tau_n)/\tau\right\}\right] = (2\pi\rho a^4 c)\, C_{LSM}/I_y. \qquad (7.1)$$

It was found that $|\tau-\tau_n|/\tau \leq 0.06$ for the experimental cases; in fact, $|\tau-\tau_n|/\tau \leq .03$ in most instances. Thus ε varied roughly as (C_{LSM}/I_x).

In the experiments circular cylinders were filled with liquid. Table 1 (page 30) shows the seven cases for which measurements were taken. The first two cases are the ones shown in Figure 8 of Reference 12: I_x was varied by adding flat metal rings around the cylinder, and corresponding changes in I_y were made by moving a counterweight to adjust the position of the center of gravity of the gyroscope. Neither I_y nor τ_n was recorded; it was necessary to estimate I_y by a process which involved application of the Stewartson-Wedemeyer theory (p. 19 of Reference 12). In the last five cases, I_x was kept constant and I_y was varied by moving a weight along a threaded shaft coinciding with the longitudinal axis of the cylinder[11]. The values of I_x and I_y used in the runs were chosen so that the empty-shell nutational frequencies, τ_n $(= I_x/I_y)$, lay in a range of values covering the eigenfrequencies C_R shown in the table. Reynolds number was varied by changing the liquids, which were silicon oils of differing viscosities. The estimated nominal values of I_y are 4.14×10^6 g cm^2 for Case 1 and 4.33×10^6 g cm^2 for Case 2. The n and k identify the inertial mode whose nondimensional frequency is C_R (=frequency/$\dot{\phi}$).

In Table 1 the nominal c/a is that value quoted in the appropriate reference[11,12]. In Reference 10 the term "fitted" c/a was introduced. As used here, fitted c/a is determined in the following way. Uncertainties in the measurement of cylinder dimensions give rise to experimental errors in c/a

TABLE 1. LIST OF EXPERIMENTAL CASES

#	Re	Fitted c/a	Nominal c/a	n, k	Ref.
1	5.20×10^{5}	3.154	3.148	1, 3	12
2	9.00×10^{3}	3.152	3.148	1, 3	12
3	5.21×10^{3}	3.140	3.126	1, 3	*
4	1.01×10^{4}	3.130	3.126	1, 3	*
5	1.24×10^{4}	1.047	1.042	1, 1	11
6	2.40×10^{3}	1.047	1.042	1, 1	11
7	1.26×10^{3}	1.047	1.042	1, 1	*

#	(Fitted c/a) C_R	ρ(g/cm^3)	I_x(g cm^2)	a (cm)
1	0.0486	0.818	Variable	3.153
2	0.0515	0.960	Variable	3.153
3	0.0495	0.972	8.23×10^{5}	4.121
4	0.0532	0.972	1.08×10^{6}	4.121
5	0.0437	0.966	7.94×10^{5}	6.359
6	0.0425	0.972	1.05×10^{6}	6.359
7	0.0415	0.974	1.05×10^{6}	6.359

* W.P. D'Amico, private communication.

which may be as large as ±1%.* Values of c/a lying within the error bound about the nominal value can therefore be used in the calculation. The fitted value is that which gives the best agreement with the data, judged subjectively. It will be seen that the $\varepsilon\tau$ vs τ relationship is extremely sensitive to c/a.

Results are presented in Figures 8-14 in the form of plots of yaw growth rate versus nutational frequency. In all cases theoretical curves are drawn for fitted values of c/a, and in two cases (Figures 10 and 12) also for the nominal c/a. It is evident from the seven cases that agreement between theory and experiment is better for the c/a ≈ 1.0 than for the c/a ≈ 3.1 cases. It is not understood why this is so; it may be related to the fact that resonance is excited for a simpler axial mode (k=1) for c/a ≈ 1.0 than for c/a ≈ 3.1, where the k=3 mode resonates.**

In Case 1, Figure 8, the two theories agree with each other at the high Reynolds number, as expected. However, the agreement with experiment is not as good as anticipated. The uncertainty in I_y previously mentioned is partly responsible. Comparison of peak locations is not possible because of lack of sufficient experimental points to delineate the maximum clearly and because of scatter in the data. In Case 2, Figure 9, discrepancies between theory and experiment are small, although percentage errors are large. In Case 3, Figure 10, the agreement is poor for the lower range of nutation rates. Overall, present theory results show better agreement with experimental data for Cases 2, 3, and 4 (Figures 9, 10, 11) than do results of the theory of Reference 10; it is expected that the two theories would disagree at lower Re.

We consider the three cases for the c/a ≈ 1.0 cylinder. For Re = 12,400, Figure 12, the data and the two theories agree quite well. For Re = 2400, Figure 13, the present theory agrees somewhat better with experiment than does the theory of Reference 10 in the prediction of $\tau\,[(\varepsilon\tau)_{max}] \equiv \tau_m$; for Re = 1260, Figure 14, it gives the better overall fit to the measurements. The results in Figures 12-14 for Re = 12,400, 2400, and 1260 show that τ_m for nominal c/a exceeds C_R by 21%, 42%, and 58% (referred to τ_m), respectively, a monotonic increase with decreasing Re. These differences are all greater than the corresponding differences for the c/a ≈ 3.1 results. The magnitude of $(\tau_m - C_R)$ provides a measure of the departure of the Stewartson-Wedemeyer approximation from our theory. The present theory and that of Reference 10, which is an improvement on the Stewartson-Wedemeyer theory, yield essentially the same results for the c/a ≈ 1.0 cases. Evidently, both c/a and Re determine the differences in the results of the two theories.

---

* *W.P. D'Amico, private communication.*

** *The mode number, k, occurs in the flow solution; see Eqs. (4.7) and (4.8).*

The calculated yaw growth rate is quite sensitive to small changes in c/a. This can be seen in Figure 10, Case 3. The nominal value of c/a gives a τ_m which is 13% less than that for the data, whereas the fitted value gives a τ_m 3% less. The calculated $(\varepsilon\tau)_{max}$ are 31% and 11% greater than the experimental maximum for the nominal and fitted values of c/a, respectively. For $3.126 < c/a < 3.140$, the calculated τ_m and $(\varepsilon\tau)_{max}$ would lie between the two curves shown in Figure 10. Thus, no choice of c/a will give a clearly superior result.

Sensitivity of the $\varepsilon\tau$ vs τ curves to changes in aspect ratio is further illustrated in Table 2 for the parameters of Case 3. The results show that a 0.8% change in c/a produces a 32% change in $(\varepsilon\tau)_{max}$ and a 13% change in τ_m. Even over this small range of c/a, both quantities depart noticeably from a linear variation. This sensitivity has important implications for the theory vis-à-vis results from laboratory experiments and field firings. With some care it is feasible to control c/a to within tolerances of, say, 0.5%, or even less, in laboratory experiments. Deformations of the cylinder would have to be accounted for; some possible causes are clamping of cylinder, compression of the liquid upon installation of the top, and temperature changes. In the experiments quoted here, it appears that c/a was known to an accuracy of ±0.5%. It is probably not feasible to control c/a to that accuracy in field firings. Typical manufacturing processes allow the internal dimensions of the cylinder to vary by much more than that. The application of the theory to such cases is then questionable.

TABLE 2. MAGNITUDE AND LOCATION OF $(\varepsilon\tau)_{max}$

c/a	$(\varepsilon\tau)_{max}$	$\tau_m \equiv \tau\,[(\varepsilon\tau)_{max}]$
3.126	1.358×10^{-4}	0.046
3.140	1.600×10^{-4}	0.050
3.150	1.788×10^{-4}	0.052

VIII. CONCLUSIONS

We have developed a method of computing the moment exerted by the spun-up liquid on the casing of a filled shell that is spinning and nutating. In addition, we are able to predict the nutational and yaw growth rates of the projectile's angular motion.

The output yields, separately and in combination, pressure and viscous shear moments on sidewall and endwalls. The applicability of the method is restricted to small angles of attack because of linearization of the Navier-

Stokes equations and to late times in the flight history because of the assumption of initially unperturbed solid-body rotation. There is, in addition, a Reynolds number limitation resulting from the presence of an error of order $O(Re^{-1})$. The permissible smallness of Reynolds number has not been definitely determined; there is an indication that it depends on the oscillation mode primarily being excited.

Limited parameter studies of moment coefficients indicated that sidewall and endwall pressure moments opposed each other and that viscous shear moment was often not negligible. Otherwise, no simple trends were discerned relating the relative contributions (sidewall, endwall, pressure, shear) to the side moment with the various parameters of the problem (Re, c/a, τ, ε).

Comparison of side moment coefficients with those of Murphy[10] showed good agreement for high Reynolds numbers, but increasing divergence with decreasing Reynolds number. For the sidewall viscous shear moment the relative discrepancies were large for Re < 1,000 (Figure 7a). However, the corresponding discrepancies in yaw growth rate were not necessarily large also. For example, the parameters of Case 1 (Figure 8), substituted into Eq. (7.1), led to the following relation between the discrepancies $\Delta(\varepsilon\tau_n)$ and $\Delta(C_{LSM})$: $\Delta(\varepsilon\tau_n) \approx 0.0012\ \Delta(C_{LSM})$.

Yaw growth rate outputs from this theory were compared with results of Murphy's theory and with measurements from gyroscope experiments. At high Re the differences between the two theories were small but increased with decreasing Re. Further experiments covering the parameter space in more detail are needed to provide a better assessment of the theory. All the experiments treated here have Re < 12,400 except for Case 1, which has an uncertainty in I_y. Thus, the most obvious need is for experimental results for Re $\geq$ 50,000. In projectile firings values of Re, up to several million are commonplace.

The sensitivity of yaw growth rate to small changes in c/a, discussed at the end of Section VII, is a significant result. This effect has been known for some time; the theories of Reference 10 and the present paper have provided a definitive demonstration of it.

ACKNOWLEDGMENTS

The authors are indebted to Miss Joan M. Bartos for programming and performing the calculations of the moments and yaw growth rates. They are also indebted to Mr. James Bradley for providing the output from Murphy's method and to Dr. William D'Amico for furnishing experimental data.

REFERENCES

1. J.T. Frasier and W.E. Scott, "Dynamics of a Liquid-Filled Shell," BRL Report No. 1391, February 1968. AD 667365.

2. Engineering Design Handbook, Liquid-Filled Projectile Design, AMC Pamphlet 706-165, April 1969. AD 853719.

3. C.W. Kitchens, Jr., N. Gerber, and R. Sedney, "Oscillations of a Liquid in a Rotating Cylinder: Part I. Solid-Body Rotation," BRL Technical Report ARBRL-TR-02081, June 1978. AD A057759.

4. K. Stewartson, "On the Stability of a Spinning Top Containing Liquid," J. Fluid Mech., Vol. 5, Part 4, September 1959, pp. 577-592.

5. E.H. Wedemeyer, "Dynamics of Liquid-Filled Shell: Theory of Viscous Corrections to Stewartson's Stability Problem," BRL Report 1287, June 1965. AD 472474.

6. E.H. Wedemeyer, "Viscous Corrections to Stewartson's Stability Criterion," BRL Report No. 1325, June 1966. AD 489687.

7. R.D. Whiting, "An Experimental Study of Forced Asymmetric Oscillations in a Rotating Liquid-Filled Cylinder," BRL Technical Report ARBRL-TR-02376, October 1981. AD A107948.

8. S. Stergiopoulos, "An Experimental Study of Inertial Waves in a Fluid Contained in a Rotating Cylindrical Cavity During Spin-Up From Rest," PhD. Thesis, York University, Toronto, Ontario, February 1982.

9. N. Gerber, R. Sedney, and J.M. Bartos, "Pressure Moment on a Liquid-Filled Projectile: Solid Body Rotation," ARBRL-TR-02422, October 1982. (ADA 120567).

10. C.H. Murphy, "Angular Motion of a Spinning Projectile With a Viscous Liquid Payload," BRL Memorandum Report ARBRL-MR-3194, July 1982. AD A118676.

11. W.P. D'Amico, Jr., and T.H. Rogers, "Yaw Instabilities Produced by Rapidly Rotating, Highly Viscous Liquids," AIAA Paper 81-0224, AIAA 19th Aerospace Sciences Meeting, St. Louis, Missouri, 12-15 January 1981.

12. R. Whiting and N. Gerber, "Dynamics of a Liquid-Filled Gyroscope: Update of Theory and Experiment," BRL Technical Report ARBRL-TR-02221, March 1980. AD A083886.

13. H. Schlichting, Boundary Layer Theory, McGraw-Hill Book Co., New York, NY, 1960.

14. W.P. D'Amico and M.C. Miller, "Flight Instability Produced by a Rapidly Spinning, Highly Viscous Liquid," Journal of Spacecraft and Rockets, Vol. 16, January-February 1979, pp. 62-64.

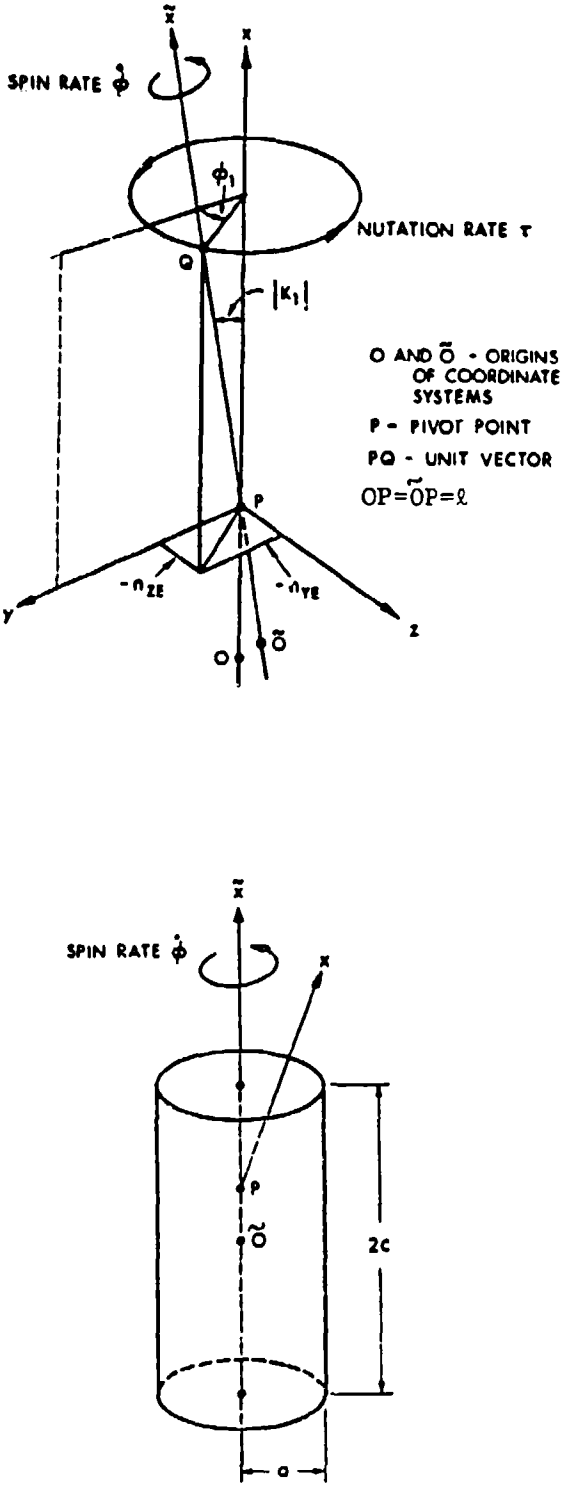

Figure 1. Diagrams of Coordinates and Cylinder.

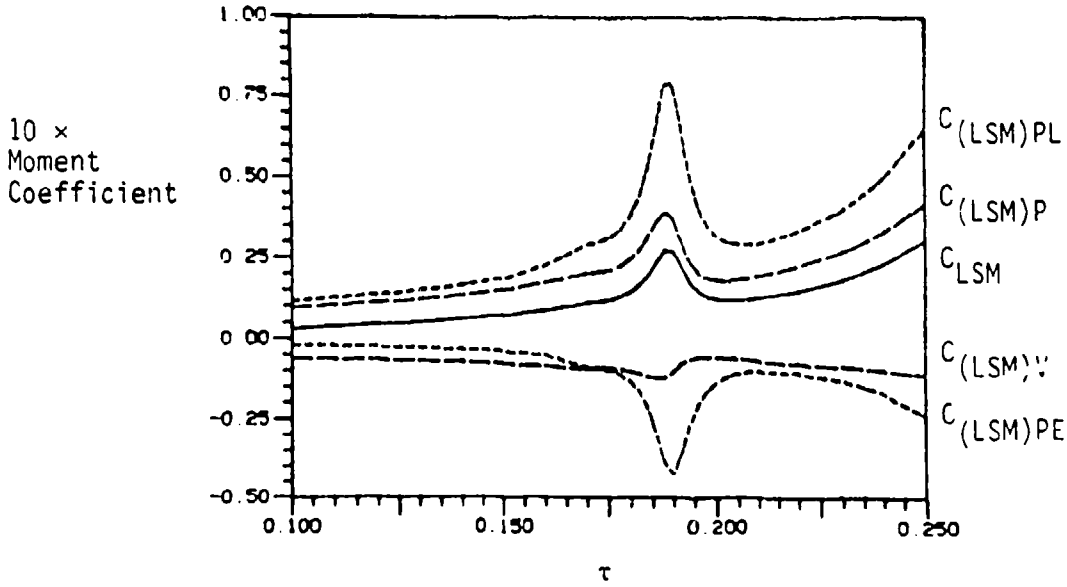

Figure 2. Pressure Moment Coefficients (Sidewall, Endwall, Total), Total Viscous Shear Moment Coefficient, and Total Moment Coefficient vs Nutational Frequency (Re=40,000, c/a=4.291, ε=0.0, i=0).

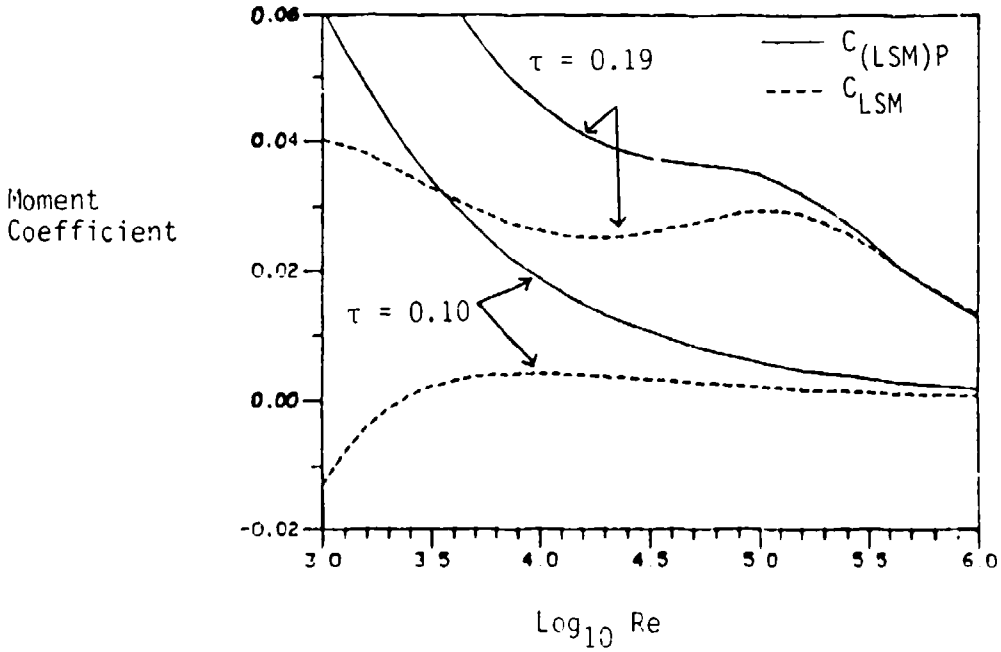

Figure 3. Variation of Pressure Side-Moment Coefficient and Total Side-Moment Coefficient with Reynolds Number for Fixed Nutational Frequency (c/a=4.291, ε=0.0, i=0).

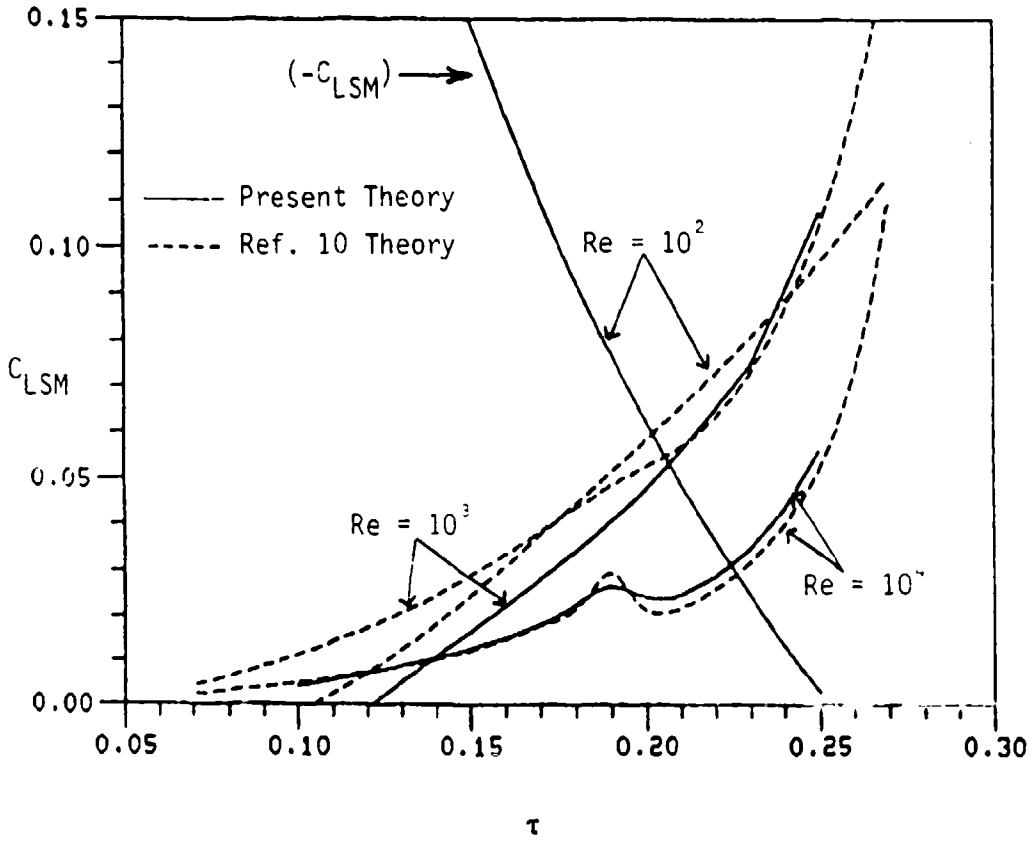

Figure 4. Total Side-Moment Coefficient vs Nutational Frequency: Comparison of Results of Reference 10 Method and Present Method (c/a=4.291, ε=0.0, i=0).

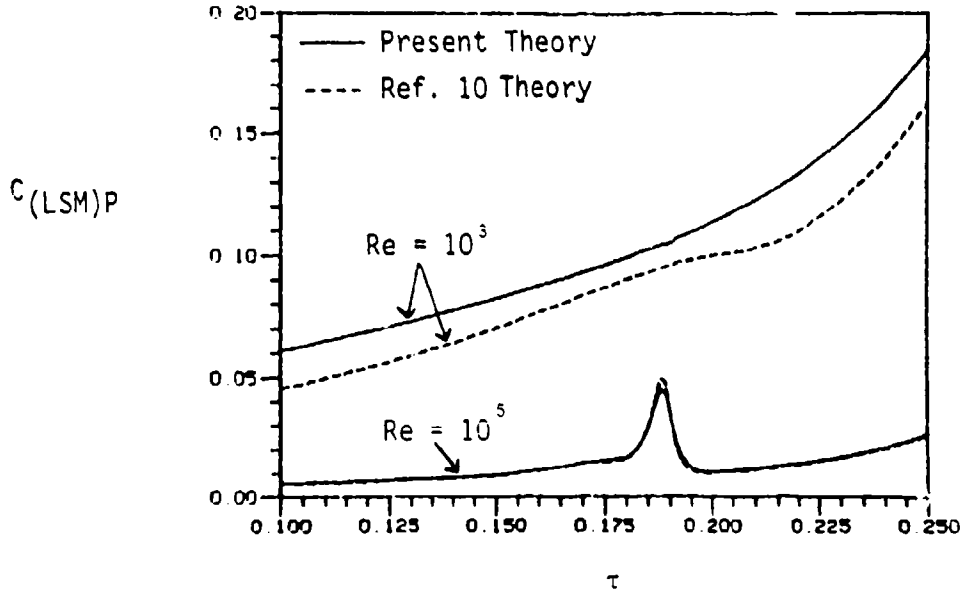

$C_{(LSM)P}$

(a)

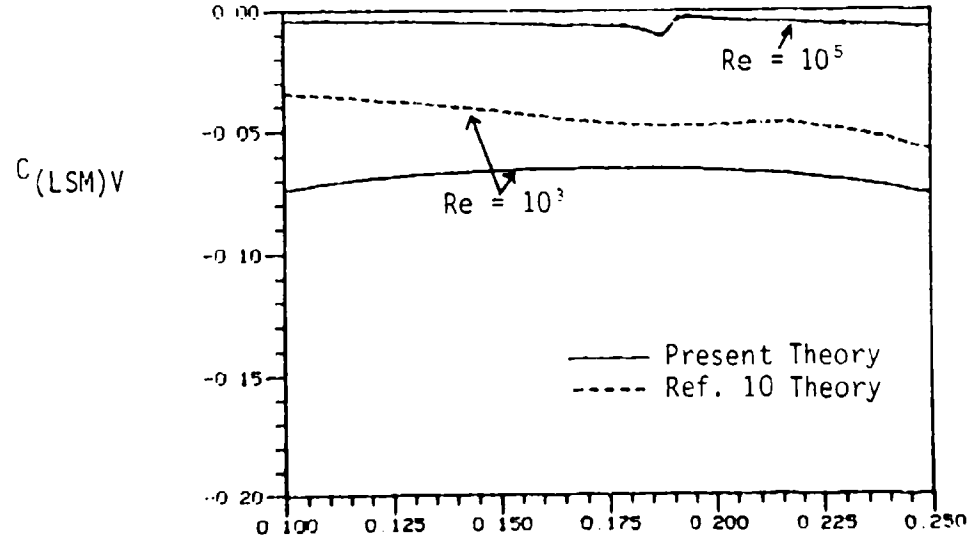

$C_{(LSM)V}$

(b)

Figure 5. Pressure and Viscous Shear Side-Moment Coefficients vs Nutational Frequency for Re = 10^3 and 10^5: Comparison of Results of Reference 10 Method and Present Method (c/a=4.291, ε=0.0, ι=0).

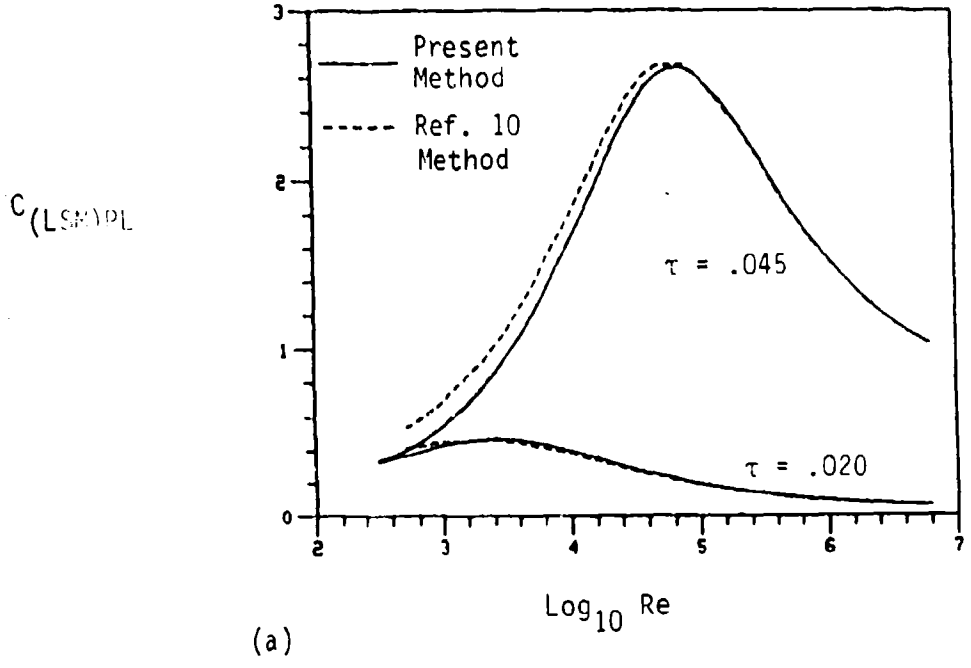

(a)

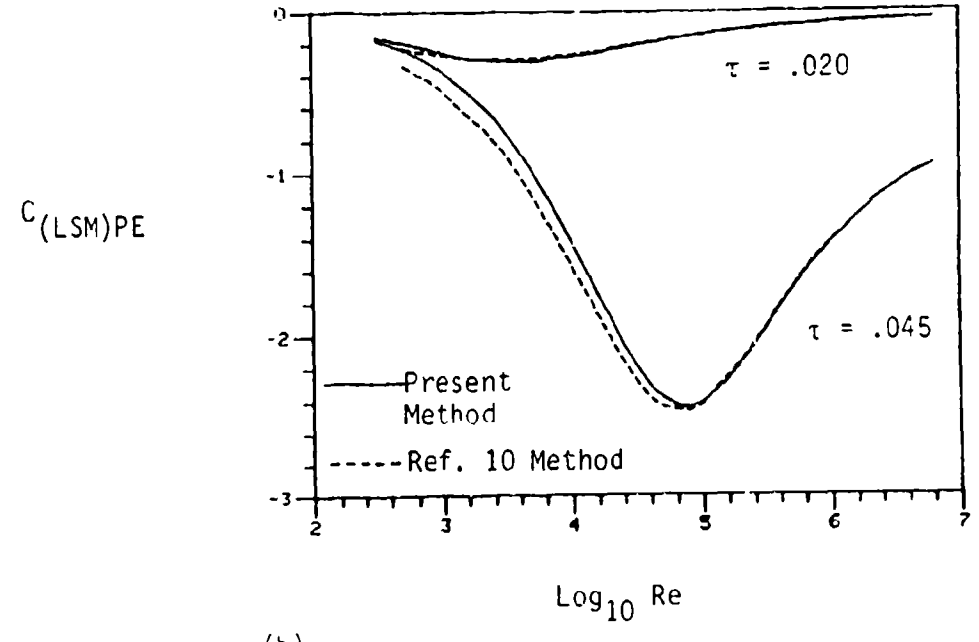

(b)

Figure 6. Pressure Side-Moment Coefficient on (a) Sidewall and (b) Endwalls: Comparison of Results of Reference 10 Method and Present Method (c/a=3.126, ε=0.02, γ=0).

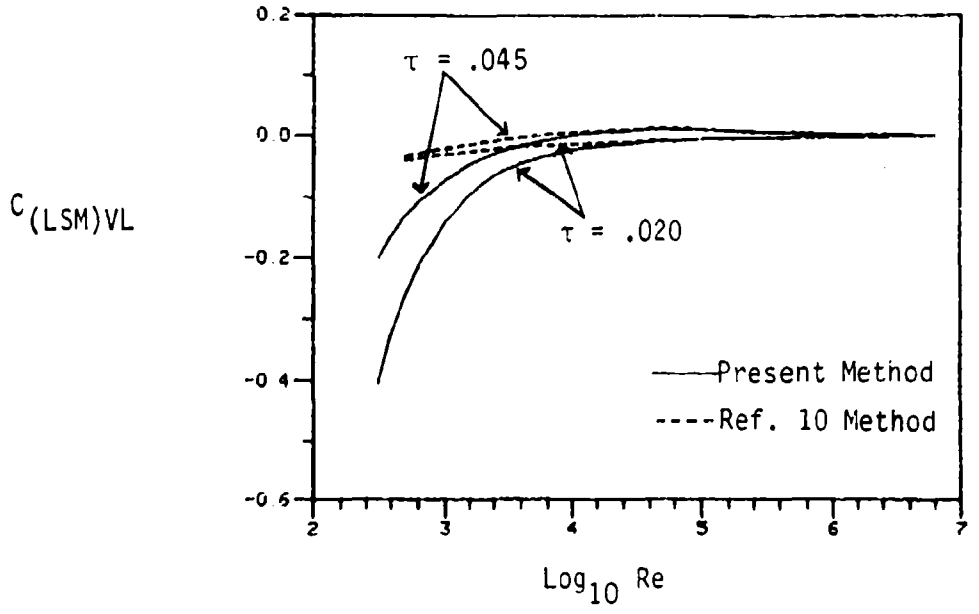

(a)

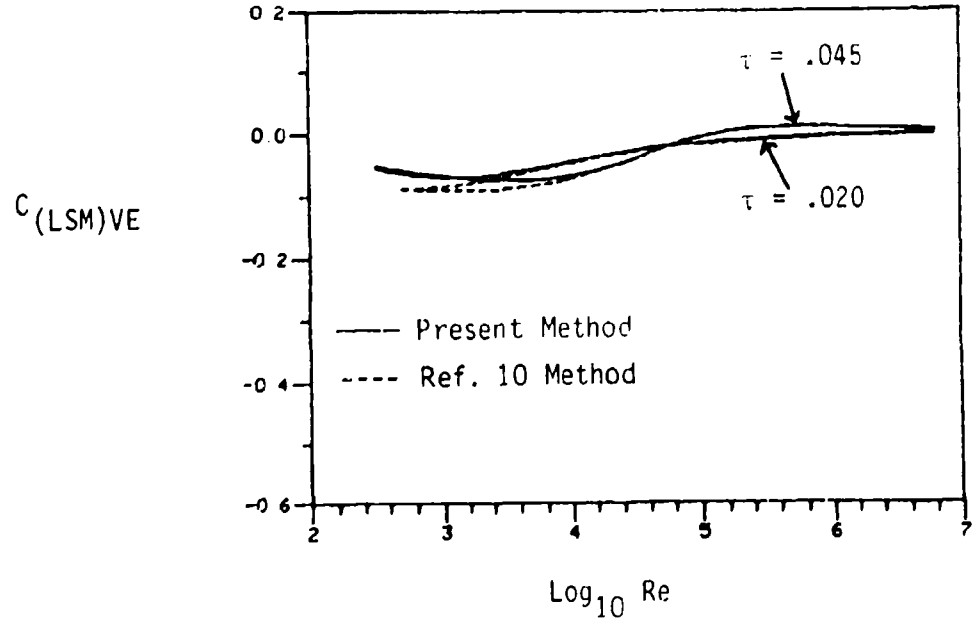

(b)

Figure 7. Viscous Shear Side-Moment Coefficient on (a) Sidewall and (b) Endwalls: Comparison of Results of Reference 10 Method and Present Method (c/a=3.126, ε=0.02, i=0).

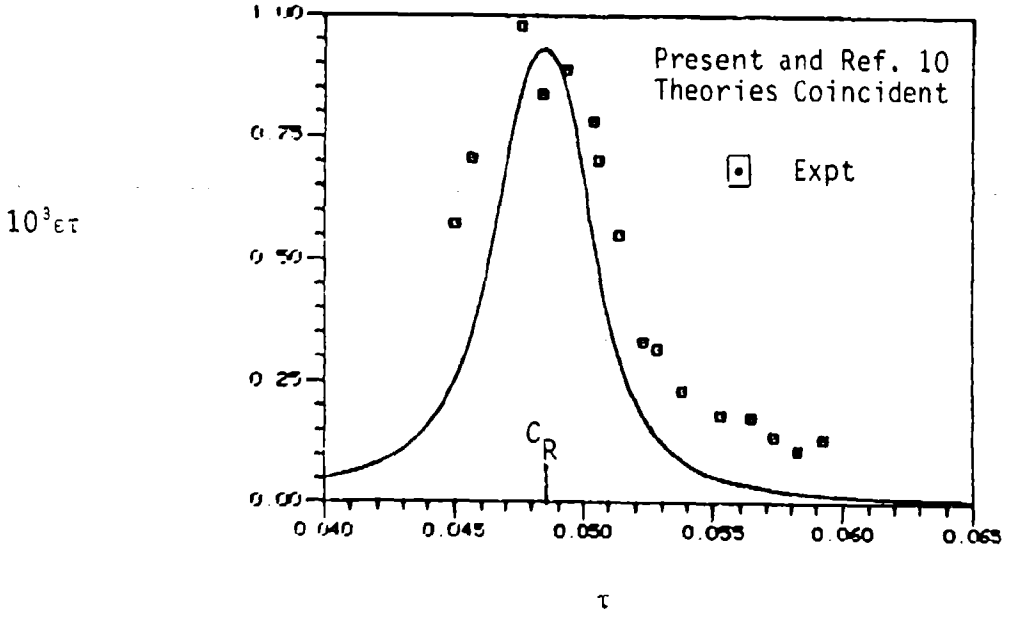

Figure 8. Yaw Growth Rate vs Nutational Frequency, Case 1: Comparison of Experimental Results with Those of Reference 10 Method and Present Method (Re = 5.20×10^5, c/a=3.154--Fitted).

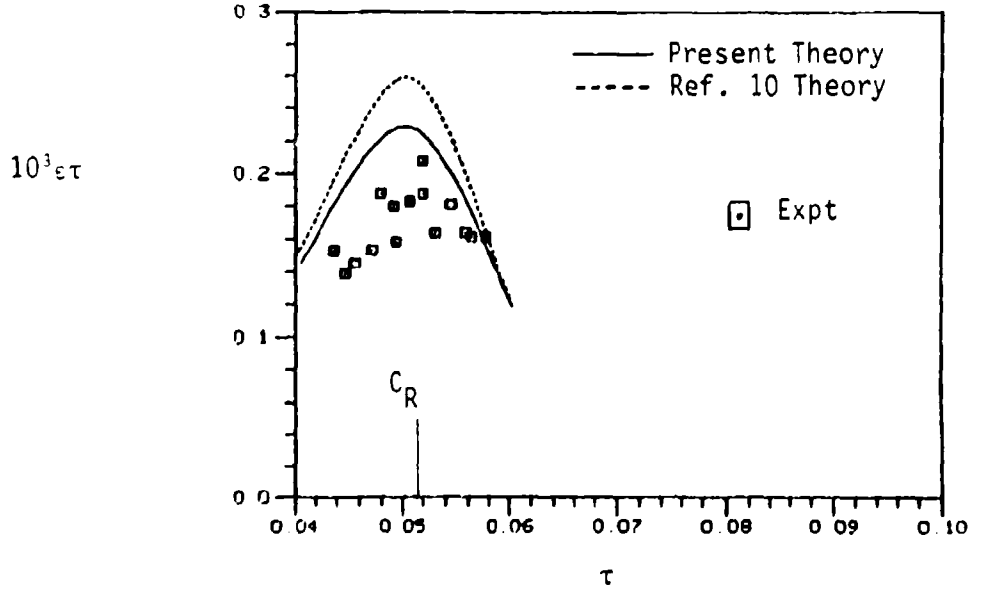

Figure 9. Yaw Growth Rate vs Nutational Frequency, Case 2: Comparison of Experimental Results with Those of Reference 10 Method and Present Method (Re = 9.00×10^3, c/a=3.152--Fitted).

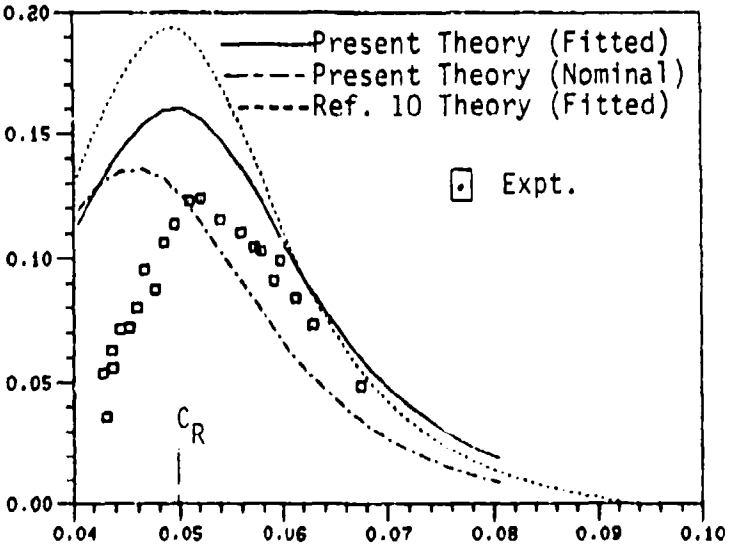

Figure 10. Yaw Growth Rate vs Nutational Frequency, Case 3: Comparison of Experimental Results with Those of Reference 10 Method and Present Method (Re = 5.21×10^3, c/a=3.140--Fitted, c/a=3.126--Nominal).

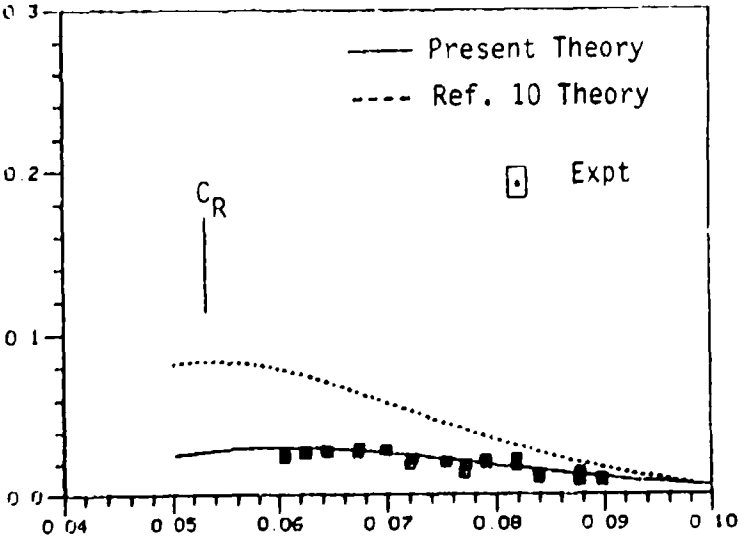

Figure 11. Yaw Growth Rate vs Nutational Frequency, Case 4: Comparison of Experimental Results with Those of Reference 10 Method and Present Method (Re = 1.01×10^3, c/a=3.130--Fitted).

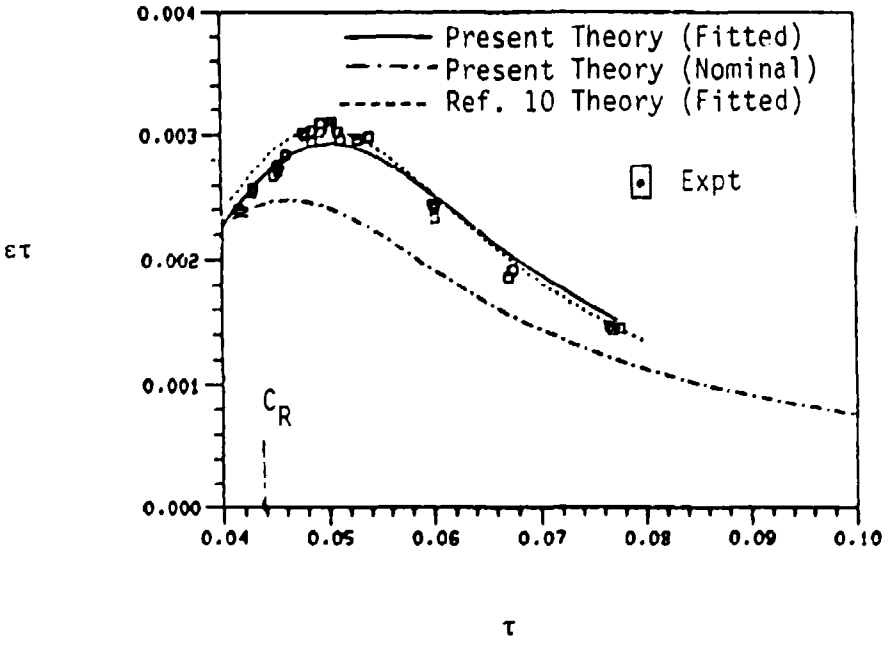

Figure 12. Yaw Growth Rate vs Nutational Frequency, Case 5: Comparison of Experimental Results with Those of Reference 10 Method and Present Method (Re = 1.24×10^4, c/a=1.047--Fitted, c/a=1.042--Nominal).

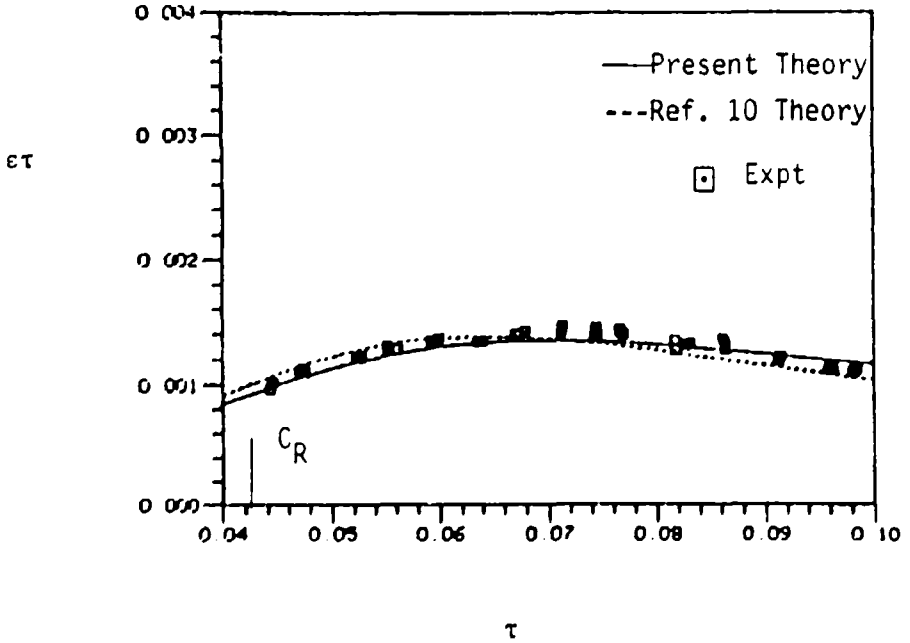

Figure 13. Yaw Growth Rate vs Nutational Frequency, Case 6: Comparison of Experimental Results with Those of Reference 10 Method and Present Method (Re = 2.40×10^3, c/a=1.047--Fitted).

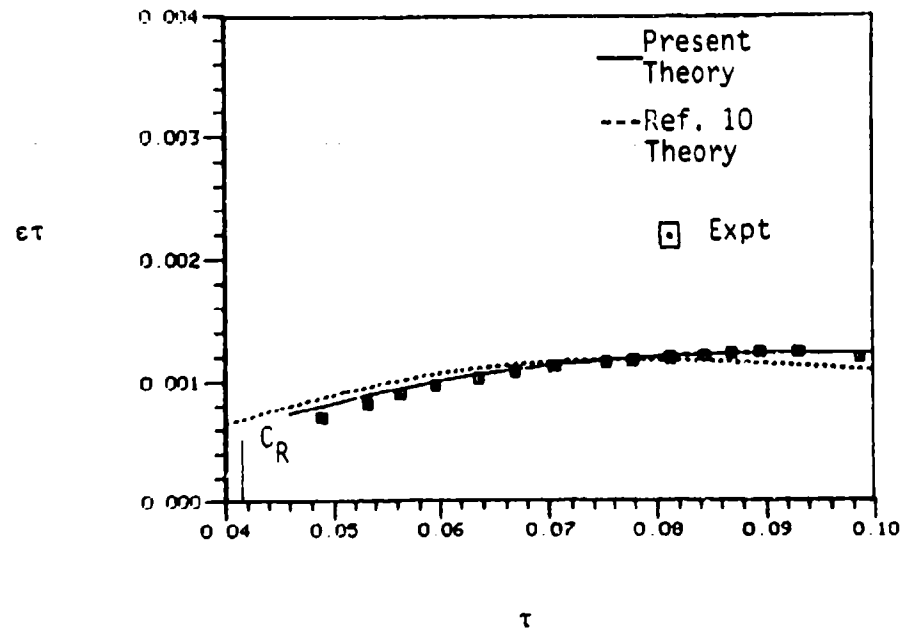

Figure 14. Yaw Growth Rate vs Nutational Frequency, Case 7: Comparison of Experimental Results with Those of Reference 10 Method and Present Method ($Re = 1.26 \times 10^3$, c/a=1.047--Fitted).

LIST OF SYMBOLS

a	cross-sectional radius of cylinder [cm]
A, B	functions of r defined in Eq. (4.12)
c	half-height of cylinder [cm]
$\bar{c}$	$\equiv c/a$, aspect ratio
C_R	natural oscillation frequency of rotating liquid/$\dot{\phi}$
C_{LM}	liquid moment coefficient = $C_{LSM} + i\, C_{LIM}$, Eq. (2.5)
C_{LIM}	liquid in-plane moment coefficient = $C_{(LIM)P} + C_{(LIM)V}$, Eq. (2.6)
C_{LSM}	liquid side moment coefficient, Eqs. (2.6) and (5.15)
$C_{(LIM)P}$	pressure in-plane moment coefficient = $C_{(LIM)PL} + C_{(LIM)PE}$
$C_{(LSM)P}$	pressure side moment coefficient, Eq. (5.14)
$C_{(LIM)V}$	viscous shear in-plane moment coefficient = $C_{(LIM)VL} + C_{(LIM)VE}$
$C_{(LSM)V}$	viscous shear side moment coefficient, Eq. (5.14)
$C_{(LIM)PE}$	endwall pressure in-plane moment coefficient, Eq. (5.13b)
$C_{(LSM)PE}$	endwall pressure side moment coefficient, Eq. (5.13a)
$C_{(LIM)PL}$	sidewall pressure in-plane moment coefficient, Eq. (5.7b)
$C_{(LSM)PL}$	sidewall pressure side moment coefficient, Eq. (5.7a)
$C_{(LIM)VE}$	endwall viscous shear in-plane moment coefficient, Eq. (5.13d)
$C_{(LSM)VE}$	endwall viscous shear side moment coefficient, Eq. (5.13c)
$C_{(LIM)VL}$	sidewall viscous shear in-plane moment coefficient, Eq. (5.7d)
$C_{(LSM)VL}$	sidewall viscous shear side moment coefficient, Eq. (5.7c)
dA	nondimensional wall surface area element, Eq. (4.20)

dF	nondimensional stress force exerted by liquid on dA [Force/$(\rho a^4 \dot{\phi}^2)$]
dF_r, dF_θ, dF_x	radial, azimuthal, and axial components, respectively, of dF [Force/$(\rho a^4 \dot{\phi}^2)$]
$dF_{\tilde{y}}$, $dF_{\tilde{x}}$	components of dF in $\tilde{y}$ and $\tilde{x}$ directions, respectively
f	$\equiv (1-i\varepsilon)\tau$, complex representation of angular motion, Eq. (2.4)
I_x	moment of inertia of empty shell about its longitudinal axis [g cm^2]
I_y	transverse moment of inertia of empty shell about its center of gravity [g cm^2]
k	index of axial eigenfunction and eigenvalue, Eqs. (4.7) and (4.9)
K_o	yaw amplitude at time t = 0
K_1	$\equiv K_o e^{\varepsilon\tau\dot{\phi}t}$, yaw amplitude at time t, Eqs. (2.3) and (2.4)
ℓ	nondimensional x (and $\tilde{x}$) coordinate of pivot point
m_L	mass of liquid in cylinder = $2\pi\rho a^2 c$ [g]
$\hat{M}$	aerodynamic (or gravity) moment parameter, Eq. (2.2)
$M_{L\tilde{Y}}$, $M_{L\tilde{Z}}$	$\tilde{y}$ and $\tilde{z}$ components, respectively, of liquid moment [g cm^2/s^2]
$M_{L\tilde{Z}B}$, $M_{L\tilde{Z}T}$	bottom and top wall contributions, respectively, to $M_{L\tilde{Z}}$ [g cm^2/s^2]
$M_{L\tilde{Z}E}$, $M_{L\tilde{Z}L}$	endwall and sidewall contributions, respectively, to $M_{L\tilde{Z}}$ [g cm^2/s^2]
n	index of radial mode for eigenfrequency, C_R
n_{YE}, n_{ZE}	components in the y, z plane of a unit vector lying on the $\tilde{x}$-axis
N_{side}	unit vector normal to sidewall; similar definition for N_{top}, Eq. (4.19)

$\underline{p} \equiv \underline{p}_R + i\,\underline{p}_I$	nondimensional r, x variation of perturbation pressure, Eq. (4.1) [pressure/$(K_o \rho a^2 \dot{\phi}^2)$]
$\underline{p}_H$	series solution contribution to $\underline{p}$ in Eq. (4.4)
p_{NS}	total pressure/$(\rho a^2 \dot{\phi}^2)$, Eq. (3.3), solution to Navier-Stokes equations
$\underline{p}_p$	particular solution contribution to $\underline{p}$, Eq. (4.3)
$\overset{*}{p}$	perturbation pressure/$(K_o \rho a^2 \dot{\phi}^2)$, Eqs. (3.3) and (4.1)
$\hat{p}_k(r)$	coefficient of $\sin \lambda_k x$ in p series, Eq. (4.7)
p	unperturbed pressure/$(\rho a^2 \dot{\phi}^2)$, Eqs. (3.3) and (3.4)
r	radial coordinate in inertial system/a
$\tilde{r}$	radial coordinate in nonrotating aeroballistic system/a
Re	Reynolds number = $a^2\dot{\phi}/\nu$
t	time [s]
u, v, w, p	nondimensional r, x variation of outer solution of flow problem
$\underline{u}, \underline{v}, \underline{w}$	nondimensional r, x variation of perturbation velocity components, Eq. (4.1) [velocity/$(K_o \dot{\phi} a)$]
$\overset{*}{u}, \overset{*}{v}, \overset{*}{w}$	nondimensional perturbation velocity components in inertial system, Eqs. (3.3) and (4.1) [velocity/$(K_o \dot{\phi} a)$]
$\overset{*}{\tilde{u}}, \overset{*}{\tilde{v}}, \overset{*}{\tilde{w}}$	nondimensional radial, azimuthal, and axial perturbation velocity components in aeroballistic system, Eq. (3.5) [velocity/$(K_o \dot{\phi} a)$]
u_C, v_C, w_C, p_C	composite solution contribution to r, x variation in flow problem, Eq. (5.16)
$\underline{u}_H, \underline{v}_H, \underline{w}_H$	series solution contribution to $\underline{u}$, $\underline{v}$, $\underline{w}$, Eqs. (4.2) and (4.4)
u_i, v_i, w_i, p_i	first term of inner solution, Eq. (D5) of Reference 9

$\hat{u}_k$, $\hat{v}_k$, $\hat{w}_k$	coefficients of sin $\lambda_k x$ and cos $\lambda_k x$ in u, v, w series, Eq. (4.7)
u_{NS}, v_{NS}, w_{NS}	nondimensional radial, azimuthal, and axial velocity components, respectively, in inertial system (Eq. (3.3)), solution to linearized Navier-Stokes equations [velocity/(ϕa)]
u_o, v_o, w_o, p_o	first term of expansion of outer solution in Eq. (D3) of Reference 9
u_o^o, v_o^o, w_o^o	first term of expansion of u_o, v_o, w_o in Eq. (D7) of Reference 9
u_{o1}, v_{o1}, w_{o1}, p_{o1}	second term of expansion of outer solution in Eq. (D3) of Reference 9
u_{o1}^o, v_{o1}^o, w_{o1}^o	first term of expansion of u_{o1}, v_{o1}, w_{o1} in Eq. (D8) of Reference 9
$\underline{u}_p$, $\underline{v}_p$, $\underline{w}_p$	particular solution contribution to $\underline{u}$, $\underline{v}$, $\underline{w}$, Eqs. (4.2) and (4.3)
$\underline{u}_R$, $\underline{u}_I$	real and imaginary parts, respectively, of $\underline{u}$ (similar definitions for $\underline{v}_R$, $\underline{v}_I$ and $\underline{w}_R$, $\underline{w}_I$, Eq. (4.2))
U, V, W	nondimensional radial, azimuthal, and axial velocity components of unperturbed flow, Eq. (3.4) [velocity/(ϕa)]
x, y, z	nondimensional rectangular coordinates in inertial system (x-axis along trajectory) [length/a]
$\tilde{x}$, $\tilde{y}$, $\tilde{z}$	nondimensional rectangular coordinates in aeroballistic system ($\tilde{x}$-axis along cylinder axis) [length/a]
y	= $\bar{\bar{c}}$ - x in Chapter IV (Eq. (4.11) et seq.)
α, β	functions of f and Re defined in Eq. (4.10)
$\tilde{\alpha}$	angle in vertical plane measured from the $\tilde{x}$-axis to the velocity vector
$\tilde{\beta}$	angle in horizontal plane measured from the $\tilde{x}$-axis to the velocity vector
δc	correction term in endwall boundary condition, Eq. (4.10)

ϵ	= $(1/\tau)$ × yaw growth per radian of nutation
θ, $\tilde{\theta}$	polar angles (azimuthal coordinates) in inertial and aeroballistic systems, respectively
λ_k	eigenvalue in the axial problem, Eqs. (4.7) and (4.9)
ν	kinematic viscosity of liquid [cm^2/s]
$\tilde{\xi}$	vector describing angular motion of cylinder, Eq. (2.1)
ρ	density of liquid [g/cm^3]
τ	nutational frequency of cylinder/$\dot{\phi}$
τ_n	nutational frequency of empty shell/$\dot{\phi}$, Eq. (2.9)
τ_{ij}	nondimensional components of stress tensor, Eq. (4.15) [stress/$(\rho a^2\dot{\phi}^2)$]
ϕ_1	= $\tau\dot{\phi}t$, angular orientation of $\tilde{x}$-axis in the x, y, z system
$\dot{\phi}$	spin rate of cylinder [rad/s], taken to be positive

DISTRIBUTION LIST

No. of Copies	Organization
12	Administrator Defense Technical Information Center ATTN: DTIC-DDA Cameron Station Alexandria, VA 22314
1	Commander US Army Engineer Waterways Experiment Station ATTN: R.H. Malter Vicksburg, MS 39181
1	Commander US Army Materiel Development and Readiness Command ATTN: DRCDMD-ST 5001 Eisenhower Avenue Alexandria, VA 22333
1	Commander US Army Armament Research and Development Command ATTN: DRDAR-TDC (Dr. D. Gyorog) Dover, NJ 07801
3	Commander US Army Armament Research and Development Command ATTN: DRDAR-TSS DRDAR-LC, Dr. J. Frasier Dover, NJ 07801
6	Commander US Army Armament Research and Development Command ATTN: DRDAR-LCA-F Mr. D. Mertz Mr. E. Falkowski Mr. A. Loeb Mr. R. Kline Mr. S. Kahn Mr. S. Wasserman Dover, NJ 07801
1	Director US Army Air Mobility Research and Development Laboratory Ames Research Center Moffett Field, CA 94035
1	Commander US Army Armament Materiel Readiness Command ATTN: DRSAR-LEP-L Rock Island, IL 61299
1	Director US Army ARRADCOM Benet Weapons Laboratory ATTN: DRDAR-LCB-TL Watervliet, NY 12189
1	Commander US Army Aviation Research and Development Command ATTN: DRDAV-E 4300 Goodfellow Blvd St. Louis, MO 63120
1	Director US Army Air Mobility Research and Development Laboratory ATTN: SAVDL-D, W.J. McCroskey Ames Research Center Moffett Field, CA 94035
1	Commander US Army Communications Research and Development Command ATTN: DRDCO-PPA-SA Fort Monmouth, NJ 07703
1	Commander US Army Electronics Research and Development Command Technical Support Activity ATTN: DELSD-L Fort Monmouth, NJ 07703
1	Commander US Army Missile Command ATTN: DRSMI-R Redstone Arsenal, AL 35898
1	Commander US Army Missile Command ATTN: DRSMI-YDL Redstone Arsenal, AL 35898

DISTRIBUTION LIST

No. of Copies	Organization
1	Commander US Army Missile Command ATTN: DRSMI-RDK, Mr. R. Deep Restone Arsenal, AL 35898
1	Commander US Army Tank Automotive Research & Development Command ATTN: DRDTA-UL Warren, MI 48090
1	Commander US Army Jefferson Proving Ground ATTN: STEJP-TD-D Madison, IN 47251
2	Commander US Army Research Office ATTN: Dr. R.E. Singleton Dr. Jagdish Chandra P.O. Box 12211 Research Triangle Park, NC 27709
1	AGARD-NATO ATTN: R.H. Korkegi APO New York 09777
1	Director US Army TRADOC Systems Analysis Activity ATTN: ATAA-SL, Tech Lib White Sands Missile Range NM 88002
3	Commander Naval Air Systems Command ATTN: AIR-604 Washington, DC 20360
2	Commander David W. Taylor Naval Ship Research & Development Center ATTN: H.J. Lugt, Code 1802 S. de los Santos, Head, High Speed Aero Division Bethesda, MD 20084
1	Commander Naval Surface Weapons Center ATTN: DX-21, Lib Br Dahlgren, VA 22448
5	Commander Naval Surface Weapons Center Applied Aerodynamics Division ATTN: K.R. Enkenhus M. Ciment S.M. Hastings A.E. Winklemann W.C. Ragsdale Silver Spring, MD 20910
1	AFATL (DLDL, Dr. D.C.Daniel) Eglin AFB, FL 32542
2	AFFDL (W.L. Hankey; J.S. Shang) Wright-Patterson AFB, OH 45433
5	Director National Aeronautics and Space Administration Ames Research Center ATTN: D.R. Chapman J. Rakich W.C. Rose B. Wick P. Kutler Moffett Field, CA 94035
4	Director National Aeronautics and Space Administration Langley Research Center ATTN: E. Price J. South J.R. Sterrett Tech Library Langley Station Hampton, VA 23365
1	Aerospace Corporation Aero-Engineering Subdivision ATTN: Walter F. Reddall El Segundo, CA 90245

DISTRIBUTION LIST

No. of Copies	Organization
1	Director National Aeronautics and Space Administration Lewis Research Center ATTN: MS 60-3, Tech Lib 21000 Brookpark Road Cleveland, OH 44135
2	Director National Aeronautics and Space Administration Marshall Space Flight Center ATTN: A.R. Felix, Chief S&E-AERO-AE Dr. W.W. Fowlis Huntsville, AL 35812
2	Director Jet Propulsion Laboratory ATTN: L.M. Mach Tech Library 4800 Oak Grove Drive Pasadena, CA 91103
3	Arnold Research Org., Inc. ATTN: J.D. Whitfield R.K. Matthews J.C. Adams Arnold AFB, TN 37389
3	Aerospace Corporation ATTN: H. Mirels R.L. Varwig Aerophysics Lab. P.O. Box 92957 Los Angeles, CA 90009
1	AVCO Systems Division ATTN: B. Reeves 201 Lowell Street Wilmington, MA 01887
3	Boeing Commercial Airplane Company ATTN: R.A. Day, MS 1W-82 P.E. Rubbert, MS 3N-19 J.D. McLean, MS-3N-19 Seattle, WA 98124
3	Calspan Corporation ATTN: A. Ritter G. Homicz W. Rae P.O. Box 400 Buffalo, NY 14225
1	General Dynamics ATTN: Research Lib 2246 P.O. Box 748 Fort Worth, TX 76101
1	General Electric Company, RESD ATTN: W.J. East 3198 Chestnut Street Philadelphia, PA 19101
2	Grumman Aircraft Corporation ATTN: R.E. Melnik L.G. Kaufman Bethpage, NY 11714
2	Lockheed-Georgia Company ATTN: B.H. Little, Jr. G.A. Pounds Dept 72074, Zone 403 86 South Cobb Drive Marietta, GA 30062
1	Lockheed Missiles and Space Company ATTN: Tech Info Center 3251 Hanover Street Palo Alto, CA 94304
3	Martin-Marietta Laboratories ATTN: S.H. Maslen S.C. Traugott H. Obremski 1450 S. Rolling Road Baltimore, MD 21227
2	McDonnell Douglas Astronautics Corporation ATTN: J. Xerikos H. Tang 5301 Bolsa Avenue Huntington Beach, CA 92647

DISTRIBUTION LIST

No. of Copies	Organization
2	McDonnell-Douglas Corporation Douglas Aircraft Company ATTN: T. Cebeci K. Stewartson 3855 Lakewood Boulevard Long Beach, CA 90801
2	Rockwell International Science Center ATTN: Dr. V. Shankar Dr. N. Malmuth 1049 Camino Dos Rios Thousand Oaks, CA 91360
3	Sandia Laboratories ATTN: F.G. Blottner W.L. Oberkampf Tech Lib. Albuquerque, NM 87115
2	United Aircraft Corporation Research Laboratory ATTN: M.J. Werle Library East Hartford, CT 06108
1	LTV Aerospace Corp. Vought Systems Division ATTN: J.M. Cooksey, Chief, Gas Dynamics Lab, 2-53700 P.O. Box 5907 Dallas, TX 75222
1	Arizona State University Department of Mechanical and Energy Systems Engineering ATTN: G.P. Neitzel Tempe, AZ 85281
1	Cornell University Graduate School of Aero Eng ATTN: Library Ithaca, NY 14850

No. of Copies	Organization
3	California Institute of Technology ATTN: Tech Library H.B. Keller Mathematics Dept. D. Coles Aeronautics Dept. Pasadena, CA 91109
1	Illinois Institute of Tech ATTN: H. M. Nagib 3300 South Federal Chicago, IL 60616
1	The Johns Hopkins University Department of Mechanics and Materials Science ATTN: S. Corrsin Baltimore, MD 21218
4	Director Johns Hopkins University Applied Physics Laboratory ATTN: Dr. R.D. Whiting Dr. D.A. Hurdif Dr. R.S. Hirsh Mr. E.R. Bohn Johns Hopkins Road Laurel, MD 20707
1	Louisiana State Univeristy Department of Physics and Astronomy ATTN: Dr. R.G. Hussey Baton Rouge, LA 70803
3	Massachusetts Institute of Technology ATTN: E. Covert H. Greenspan Tech Lib 77 Massachusetts Avenue Cambridge, MA 02139

DISTRIBUTION LIST

No. of Copies	Organization
2	North Carolina State Univ Mechanical and Aerospace Engineering Department ATTN: F.F. DeJarnette J.C. Williams Raleigh, NC 27607
1	Northwestern University Department of Engineering Science and Applied Mathematics ATTN: Dr. S.H. Davis Evanston, IL 60201
1	Notre Dame University Department of Aero Engr ATTN: T.J. Mueller South Bend, IN 46556
2	Ohio State University Dept of Aeronautical and Astronautical Engineering ATTN: S.L. Petrie O.R. Burggraf Columbus, OH 43210
2	Polytechic Institute of New York ATTN: G. Moretti S.G. Rubin Route 110 Farmingdale, NY 11735
3	Princeton University James Forrestal Research Ctr Gas Dynamics Laboratory ATTN: S.M. Bogdonoff S.I. Cheng Tech Library Princeton, NJ 08540
1	Purdue University Thermal Science & Prop Ctr ATTN: Tech Library W. Lafayette, IN 47907
1	Rensselaer Polytechnic Institute Department of Math Sciences ATTN: R.C. Diprima Troy, NY 12181
1	University of California Davis ATTN: H. A. Dwyer Davis, CA 95616
1	San Diego State University Department of Aerospace Engr and Engineering Mechanics College of Engineering ATTN: K.C. Wang San Diego, CA 92182
1	Southern Methodist University Department of Civil and Mechanical Engineering ATTN: R.L. Simpson Dallas, TX 75275
1	Southwest Research Institute Applied Mechanics Reviews 8500 Culebra Road San Antonio, TX 78228
6	Stanford University Dept of Aeronautics/Astronautics ATTN: Dr. J.L. Steger (3 cys) Dr. S. Chakravarthy (3 cys) Stanford, CA 94305
1	Texas A&M University College of Engineering ATTN: R.H. Page College Station, TX 77843

DISTRIBUTION LIST

No. of Copies	Organization
1	University of California - Berkeley Department of Aerospace Engineering ATTN: M. Holt Berkeley, CA 94720
2	University of California - San Diego Department of Aerospace Engineering and Mechanical Engineering Sciences ATTN: P. Libby Tech Library La Jolla, CA 92037
1	University of Cincinnati Department of Aerospace Engineering ATTN: R.T. Davis Cincinnati, OH 45221
1	University of Colorado Department of Astro-Geophysics ATTN: E.R. Benton Boulder, CO 80304
2	University of Maryland ATTN: W. Melnik J.D. Anderson College Park, MD 20740
1	University of Maryland - Baltimore County Department of Mathematics ATTN: Dr. Y.M. Lynn 5401 Wilkens Avenue Baltimore, MD 21228
1	University of Santa Clara Department of Physics ATTN: R. Greeley Santa Clara, CA 95053
2	University of Southern California Department of Aerospace Engineering ATTN: T. Maxworthy P. Weidman Los Angeles, CA 90007
2	University of Michigan Department of Aeronautical Engineering ATTN: W.W. Wilmarth Tech Library East Engineering Building Ann Arbor, MI 48104
2	University of Rochester Department of Mechanical and Aerospace Sciences ATTN: R. Gans A. Clark, Jr. Rochester, NY 14627
1	University of Tennessee Department of Physics ATTN: Prof. W.E. Scott Knoxville, TN 37916
1	University of Texas Department of Aerospace Engineering ATTN: J.C. Westkaemper Austin, TX 78712
1	University of Virginia Department of Aerospace Engineering & Engineering Physics ATTN: I.D. Jacobson Charlottesville, VA 22904
1	University of Virginia Research Laboratories for the Engineering Sciences ATTN: Prof. H. G. Wood P.O. Box 3366 University Station Charlottesville, VA 22903

DISTRIBUTION LIST

No. of Copies	Organization
1	University of Washington Department of Mechanical Engineering ATTN: Tech Library Seattle, WA 98105
1	University of Wyoming ATTN: D.L. Boyer University Station Laramie, WY 82071
3	Virginia Polytechnic Institute and State University Department of Aerospace Engineering ATTN: Tech Library Dr. W. Saric Dr. T. Herbert Blacksburg, VA 24061
1	Woods Hole Oceanographic Institute ATTN: J.A. Whitehead Woods Hole, MA 02543

No. of Copies	Organizatio
	Aberdeen Proving Ground
	Director, USAMSAA ATTN: DRXSY-D DRXSY-MP, H. Cohen
	Commander, USATECOM ATTN: DRSTE-TO-F
	Director, USACSL, Bldg. E3330, EA ATTN: Munitions Division W.C. Dee
	Director, USACSL, Bldg. E3516, EA ATTN: DRDAR-CLB-PA M. Miller

USER EVALUATION OF REPORT

Please take a few minutes to answer the questions below; tear out this sheet, fold as indicated, staple or tape closed, and place in the mail. Your comments will provide us with information for improving future reports.

1. BRL Report Number _____

2. Does this report satisfy a need? (Comment on purpose, related project, or other area of interest for which report will be used.)

_____

_____

_____

3. How, specifically, is the report being used? (Information source, design data or procedure, management procedure, source of ideas, etc.) _____

_____

_____

4. Has the information in this report led to any quantitative savings as far as man-hours/contract dollars saved, operating costs avoided, efficiencies achieved, etc.? If so, please elaborate.

_____

_____

5. General Comments (Indicate what you think should be changed to make this report and future reports of this type more responsive to your needs, more usable, improve readability, etc.) _____

_____

_____

_____

6. If you would like to be contacted by the personnel who prepared this report to raise specific questions or discuss the topic, please fill in the following information.

Name: _____

Telephone Number: _____

Organization Address: _____

_____

_____